ATTACHMENT J.4.44

SILO 3 MATERIAL COMPOUND ANALYSIS

ARGONNE NATIONAL LABORATORY (8/04/97)

ARGONNE NATIONAL LABORATORY
9700 South Cass Avenue
Argonne, Illinois 60439

SILO 3 MATERIAL COMPOUND ANALYSIS

FINAL REPORT

October 10, 1997

E. C. Buck
S. F. Wolf

CHEMICAL TECHNOLOGY DIVISION

SILO 3 MATERIAL COMPOUND ANALYSIS
FINAL REPORT

by
Edgar C. Buck and Steven F. Wolf

Chemical Technology Division, Argonne National Laboratory

ABSTRACT

This report describes results and data interpretations obtained between March and June 1997 as part of the characterization task for Fluor Daniel Fernald. A combination of wet chemical analysis, optical microscopy, scanning electron microscopy with backscattered electron imaging, and analytical transmission electron microscopy were used to characterize the structure and composition of the Silo 3 material from the former uranium processing facility at Fernald, OH.

The dominant phases in the Silo 3 material have been identified, as anhydrite ($CaSO_4$), iron sulfate, fairfieldite group Mg-phosphates, hematite (Fe_2O_3), turquoise-group Fe-phosphates, and quartz (SiO_2). These phases account for nearly all the sulfur, phosphorus, magnesium, iron, and silicon in the material.

BACKGROUND

This report describes the results and data interpretations obtained on the Silo 3 material for Fluor Daniel of Fernald, Ohio. The sample was sent to Argonne National Laboratory by R. Slagle of Nuclear Fuel Services, Inc., Erwin, TN. Fluor Daniel Fernald is planning the remediation of the Silo 3 waste, which is classified as a by-product material, as defined by Section 11(e)2 of the Atomic Energy Act of 1954, as amended. Compound analysis of the Silo 3 material will assist in the immobilization development. We have used a combination of wet chemical analysis with inductively coupled plasma - mass spectrometry (ICP-MS), X-ray diffraction (XRD), scanning electron microscopy (SEM) with backscattered electron (BSE) imaging, and analytical transmission electron microscopy (AEM) to characterize the structure and composition of the compounds present in the Silo 3 material.

The methodology employed in this study goes beyond the standard approach for the analysis of soils and environmental samples adopted by the Environmental Protection Agency (EPA) (EPA,1992; NEIHESEL, 1992). The soil was first examined with SEM combined with elemental analysis with EDS. This technique provided a general view of the composition and microstructure. With AEM, the sub-micrometer particles could be determined uniquely. This would not have been possible with only SEM and XRD. Although other characterization techniques are available for probing local structure, such as X-ray absorption spectroscopy, Raman spectroscopy, and nuclear magnetic resonance, these methods do not possess the wide utility of the chosen methods. However, these methods would further enhance the characterization study. The microscopic characterization tools were used only to provide compositions of the likely compounds. The quantitative compound analysis was then derived with the aid of the elemental wet chemical analysis. Owing to the time constraints and level of effort, this work can not be considered as complete as other characterization studies performed at Fernald, such as those performed for the DOE Uranium in Soils Demonstration Program. Therefore, this study remains a semi-quantitative analysis of the Silo 3 samples.

DOCUMENTATION

Complete records of the experimental procedures followed in the examination of the Silo 3 material with electron microscopy and X-ray diffraction are recorded in scientific notebooks #1160 and #1429.

I. SCANNING ELECTRON MICROSCOPY INVESTIGATION

Scanning electron microscopy (SEM) is a well established method for investigating the nature of environmental samples, such as soils and residues. The ease of sample preparation and interpretation of data has made it an instrument of choice for many laboratories engaged in characterization studies. The technique can rapidly provide information on the distribution of major components in the sample.

In this study, we used the SEM to determine the general composition, to provide information on the basic form of the sample, and to determine whether we could use the microscope to provide representative sampling information from the provided sample. In the case of the last point, we found that there were some problems with the heterogenity of the sample; however, the method employed to determine the compound distribution, was designed to eliminate these problems.

BACKGROUND

Scanning electron microscopy was used to determine the composition of particles from the sample. As polished cross-sections of the material were used, the technique enabled observation of the particles' form. In SEM, the sample is exposed to an electron beam which rasters rapidly across the surface. The electron beam undergoes a number of events when it hits the sample, including characteristic X-ray production (GOLDSTEIN and JOY, 1986) and backscattered electrons (LORETTO, 1984). The X-rays are used to determine the composition of the material and the intensity of the backscattered electron signal is proportion to the square of the average atomic number of the material probed. The SEM images of the Silo 3 material highlight the regions of higher average atomic number. For example, lead oxide particles will be more prominent (or visible) than magnesium phosphate particles. The effect of Z-contrast must be accounted for when interpreting the backscatted images in this study.

DOCUMENTATION

Complete records of the experimental procedures followed in the examination of the Silo 3 material with scanning electron microscopy are recorded in scientific notebook #1160.

SYSTEM DESCRIPTION

Sample characterization was performed on a Topcon ABT-60 SEM equipped with a Robinson backscattered detector and a Noran Instruments Voyager 3 X-ray microanalysis system consisting of an ultra-thin window X-ray detector and digital pulse processor.

CALIBRATION

Calibration of the spectral energy peaks to the corresponding input X-ray energies is achieved by matching the energy of a pure and clean copper standard to reportedly known values. The Noran Voyager calibration programs were used to correct spectra for shifts in energy.

SAMPLE PREPARATION

Samples of the Silo 3 material were embedded in a range of epoxy resins (BUCK et al., 1995). For later TEM observation, LR white and TEM polyester resins were used. To avoid removal of the heavier components during polishing, the SEM sample mount was cut in half and polished on one of the cut surfaces. Fractionation of particles was observed in the cross-sections. Transmission microscopy samples were taken from different regions of the LR white blocks, so that different types of particles could be obtained.

SCANNING ELECTRON MICROSCOPY RESULTS

The object of the scanning electron microscopy study was to obtain very genera information on the sample. The images indicate the morphology and distribution of compounds in the Silo 3 material.

Scanning electron microscopy revealed that the Silo 3 material consisted of agglomerates of fine-grained material. In Figures I.1 through I.6, show a series of SEM/BSE images which illustrates the variety of particle morphologies found in the Silo 3 material. An effort was made to determine the composition of the material with X-ray energy dispersive spectroscopy (EDS) (see Table. I.1). As large an area as possible was analyzed; however the results did confirm that representative samples of the individual phases were obtained for the AEM examination. The EDS analyses of the sample suggested that the major phases were magnesium-, phosphorus- and sulfur-bearing, and silicon oxide. Owing to the small size of the particles, it was not possible to extract much more information on the composition of individual particles. Note that Cl peak, which appears in the SEM-EDS analyses, is from the epoxy resin. It would have been preferable if the SEM-EDS and wet chemical analyses were identical. These analyses demonstrate, that there is a significant degree of heterogenity in the Silo 3 material and that the microscopic quantification may not be examining all phases in the sample.

The identification of actinide-bearing particles in the Silo 3 material was also difficult due to their sub-micron nature. Although the SEM provided important representative information on the overall form of particles in the sample, including their morphology, a more sensitive technique was required to determine the exact form of the particles.

Table I.1 Analysis of Silo 3 material with SEM X-ray energy dispersive spectroscopy.

El	trial 1	trail 2	trail 3	trail 4	trail 5	SEM - EDS
Mg	15.9	22.5	5.0	11.5	14.1	**16.8**
Al	7.5	7.0	9.5	17.6	9.2	**11.2**
Si	20.9	14.2	51.5	23.6	24.2	**24.5**
P	25.5	26.8	15.5	11.7	16.4	**20.0**
S	10.5	7.5	6.2	13.7	13.0	**9.0**
Ca	8.2	9.9	3.1	9.1	10.4	**7.3**
Fe	7.6	6.9	6.9	9.0	9.5	**6.4**

[1]SEM quantification was based on normalized abundance's of the major detectable species. Errors are based on counting statistics.

[2]Data reported by R. Slagle of Nuclear Fuel Services, Inc. normalized to the elements reported in the SEM study (i.e. the reported values are not absolute concentrations).

There was a major discrepancy between the wet chemical results and those obtained with SEM/EDS. In particular, the levels of Na, S, and Fe are underestimated by the EDS method and the values for P, Si, and Al are overestimated. This may be due to problems in the quantification method; however, it is the variation between EDS analyses which is most significant. The variation in the determined compositions suggests in homogenity on a scale larger than the SEM can easily analyze. As we did not use the SEM to determine the composition of the material (this was determined with the wet chemical analysis), this is not considered to be deterimental to the study. The SEM was used to obtain very general compositions ranges for the major components of the Silo 3 material. The technique was also used to confirm that the AEM samples came from representative regions. The EDS method was also unable to report values for nitrogen and carbon which are major components in the Silo 3 material. This remains a problem with the complete analysis. We do not have good information on the form of nitrogen- and carbon-bearing phases.

Fig. L1 Backscattered SEM image of Silo 3 material and EDS analyses. Magnesium and iron phosphates dominate as the major components.

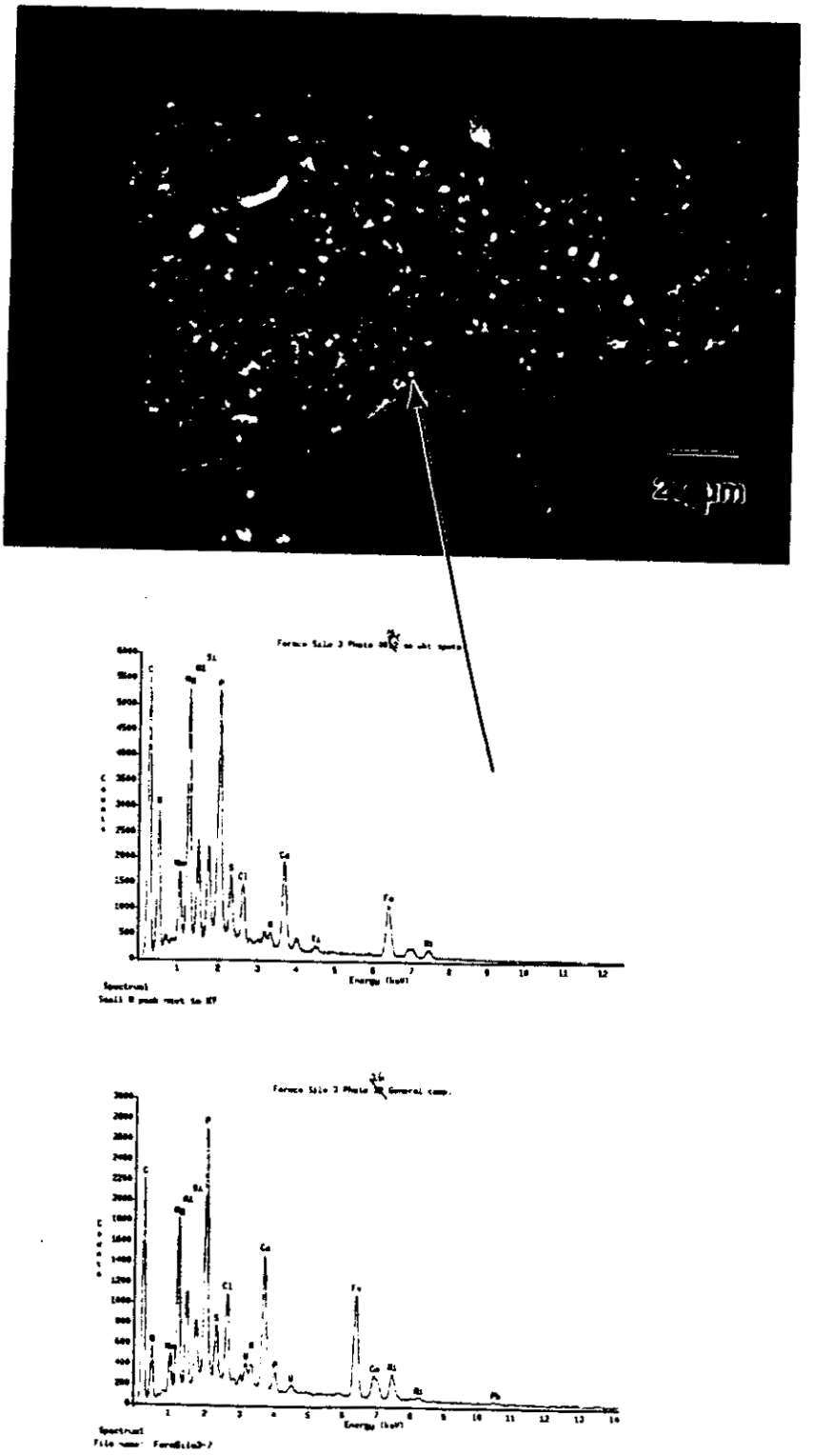

Fig. I.2 Backscattered SEM images of Silo 3 material and EDS analyses. The EDS analyses of the small white particles indicated the presence of lead and zirconium-bearing phases with a matrix of phosphate material.

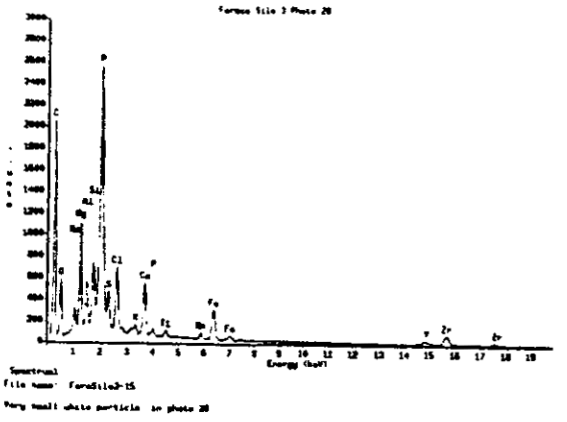

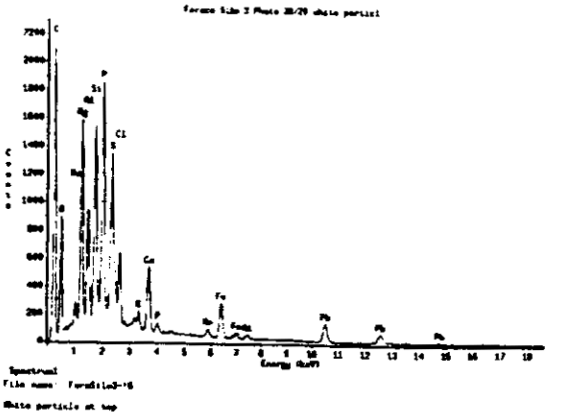

Fig. I.3 Backscattered SEM images of Silo 3 material and EDS analyses. The quartz particle which is the major phase in the image area appears to be pitted. At its edge rare earth and an actinide-bearing vanadate were found. All of these phases were also found during the TEM examination. The high Z material appears brighter in the backscattered image.

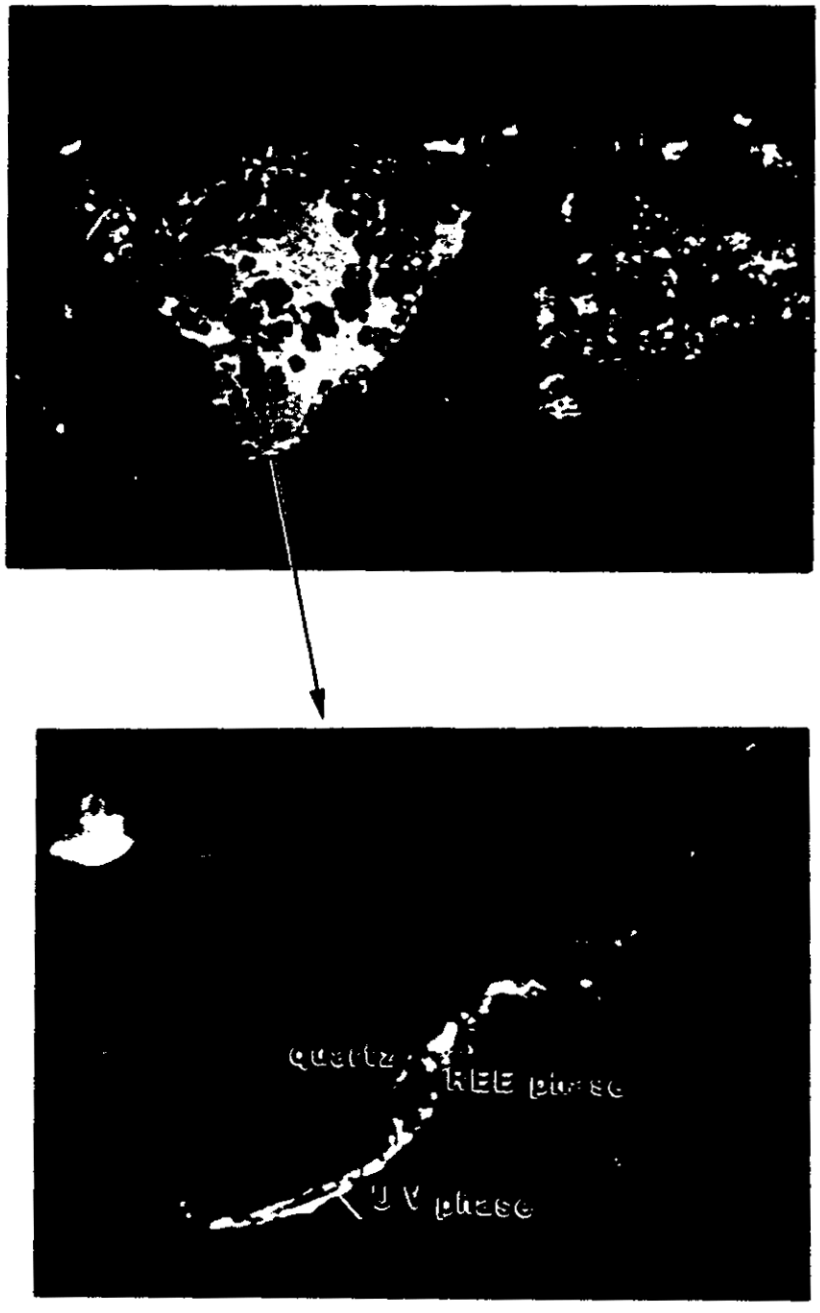

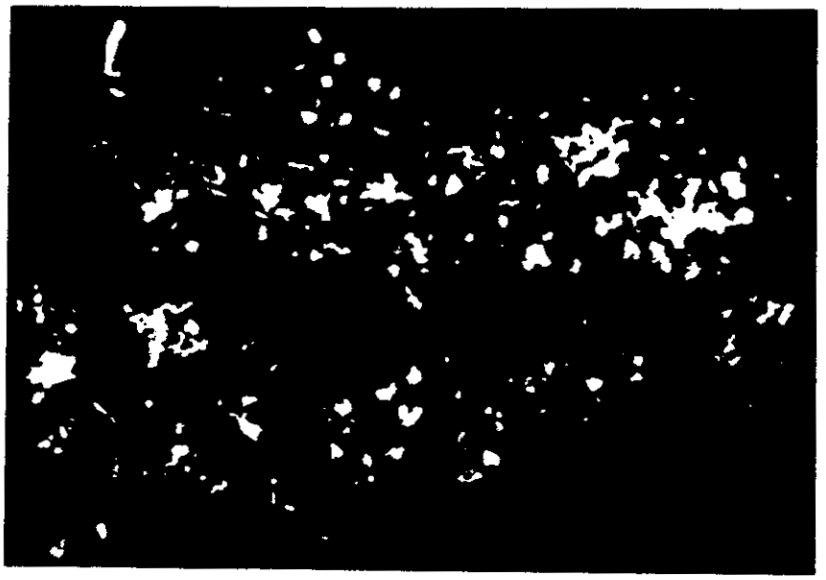

Fig. I.4 Backscattered SEM images of Silo 3 material and EDS analyses. Although under the optical microscope, the material was relatively uniform , at the SEM level, the morphology of the particles varied a great deal.

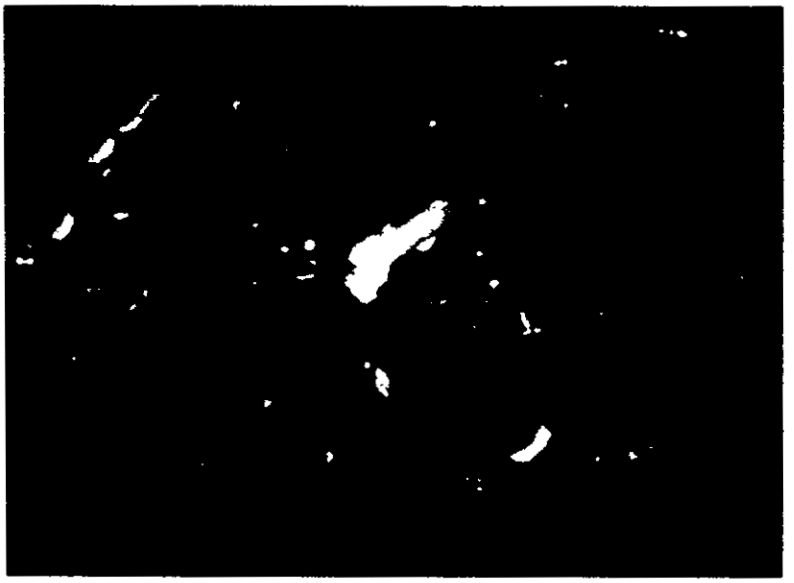

Fig. I.5 Backscattered SEM images of Silo 3 material and EDS analyses.

Fig. I.6 Backscattered SEM images of Silo 3 material and EDS analyses. The particles in this image were mainly phosphates. The bright particle towards the top left maybe cassiterite (SnO_2).

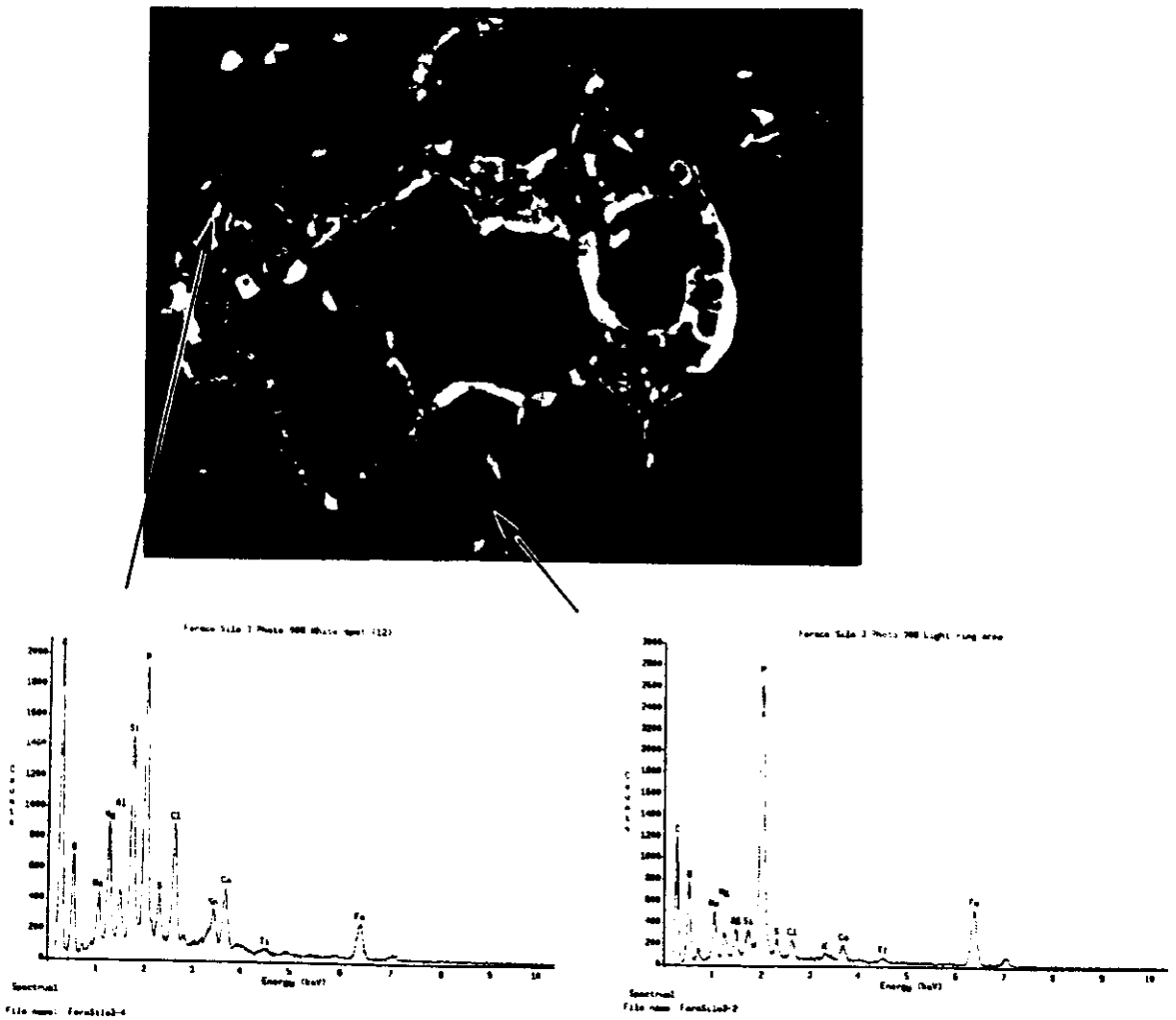

In Fig. I.7, a low magnification image of the Silo 3 material shows the form of the particles. The composition of these individual agglomerates varied only slightly, with the concentrations of the major elements, Mg, Al, Si, P, and S relatively constant. Tests with sample preparation techniques indicated that there was some size and density fractionation of particles during the curing. In order to eliminate this effect, cross sections of the mounted materials were taken. This was also important during the TEM sample preparation. In this case, the problem was overcome by using different sample preparation methods.

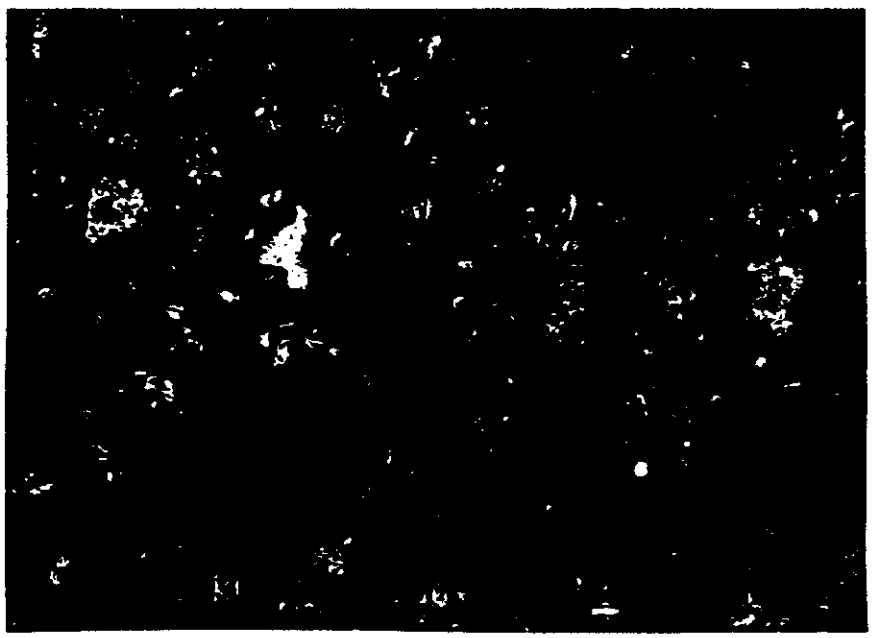

Fig. I.7 Low Magnification Backscattered Image of Particles from Silo 3 Material.

II. ANALYTICAL TRANSMISSION ELECTRON MICROSCOPY INVESTIGATION

The analytical transmission electron microscopy (AEM) study is considered to be one of the most important components of this study because information from the AEM was used to detemermine the exact form of the compounds in the Silo 3 material. The AEM was not used to determine the reative amounts of phases. It was used only to identify the individual phases.

BACKGROUND

From the initial surveys of the Silo 3 material with electron microscopy, it was apparent that the material contained a large number of sub-micrometer particles and that any assessment of the distribution of compounds within this sample would require an analytical transmission electron microscopy (AEM) study. The AEM technique provided sufficient resolution to probe the composition and structure of the numerous phases present in the Silo 3 material, as well as the small actinide-bearing phases which were contained within a matrix of other components. The object of the AEM study was to determine all the structures of all compounds in the material and provide a rough estimate of their distribution. This information would be used to interpret the X-ray diffraction analysis, so that the distribution of phases could be determined.

Transmission electron microscopy provides both image and diffraction information from the same small sample volume, typically < 1μm (LORETTO, 1984). Unlike SEM, the electron beam must pass through the sample and as electrons interact strongly with matter, it is necessary to use an extremely thin sample, usually 30-50 nm thick. This strong interaction causes characteristic X-ray production, like in the scanning microscope, and so with the appropriate detectors, compositional information can be obtained. The instrument used in this study also had an attached electron energy loss spectrometer, which was used to investigate the light elements in the sample (EGERTON, 1986). Unlike X-rays, the strong interaction means that amorphous materials can be imaged as easily as crystalline phases.

DOCUMENTATION

Complete records of the experimental procedures followed in the examination of the Silo 3 material with analytical transmission electron microscopy are recorded in scientific notebook #1429.

SYSTEM DESCRIPTION

The AEM examinations were carried out with a JEOL 2000 FXII instrument operated at 200 kV and equipped with X-ray energy dispersive spectroscopy (EDS) and electron energy loss spectroscopy (EELS). The EDS analyses were performed with both a Be-window detector,

termed the high-take-off (HTA) detector, and an ultra-thin window (UTW) detector. The Be-window prevents detection of X-rays below around 1 keV, whereas the UTW detector can detect X-rays as low as about 200 eV (including oxygen, nitrogen, and carbon). Some images were collected with a slow scan Charged Coupled Device (CCD) camera. Quantification of EDS analysis was performed with experimentally determined *k*-factors obtained from glass and mineral thin-film standards and with the aid of analysis software from the National Institute of Standards and Technology (NIST). Phases were identified by a combination of EDS, EELS, and electron diffraction.

CALIBRATION

Magnification calibration was achieved with a NIST traceable carbon replica. The diffraction calibration was achieved with a standard aluminum oxide powdered sample. Both the magnification and camera length calibrations are carried out annually. Calibration of the spectral energy peaks to the corresponding input X-ray energies was achieved by matching the energy of a pure and clean copper standard to known values. Quantification of EDS analysis was achieved with the NIST DTSA computer package (GOLDSTEIN and JOY, 1986). All TEM-EDS analyses have a Cu-K_{α} peaks caused by fluorescence from the copper support grid. The detection of copper can be difficult unless it is present in significant amounts.

SAMPLE PREPARATION

The Silo 3 samples were prepared for AEM examination by two methods. One technique involved mixing the material with LR White acrylic resin. The resin was cured at 60°C inside a polyethylene vial. The cured block was trimmed and thin sectioned with an ultramicrotome. In the other technique, the samples of Silo 3 material were crushed under acetone and deposited on a "holey" carbon grid. The first technique allowed the spatial relationships between particles in the sample to be preserved, while the second method provided a rapid method for determining the composition range and distribution of particles in the sample. These techniques are commonly used to examine environmental samples containing colloidal-sized particles (BUFFLE and LEPPARD, 1995).

The figure below shows a low magnification image of a thin section of the Silo 3 material. The AEM allows the observation of the unique particle morphology of this material.

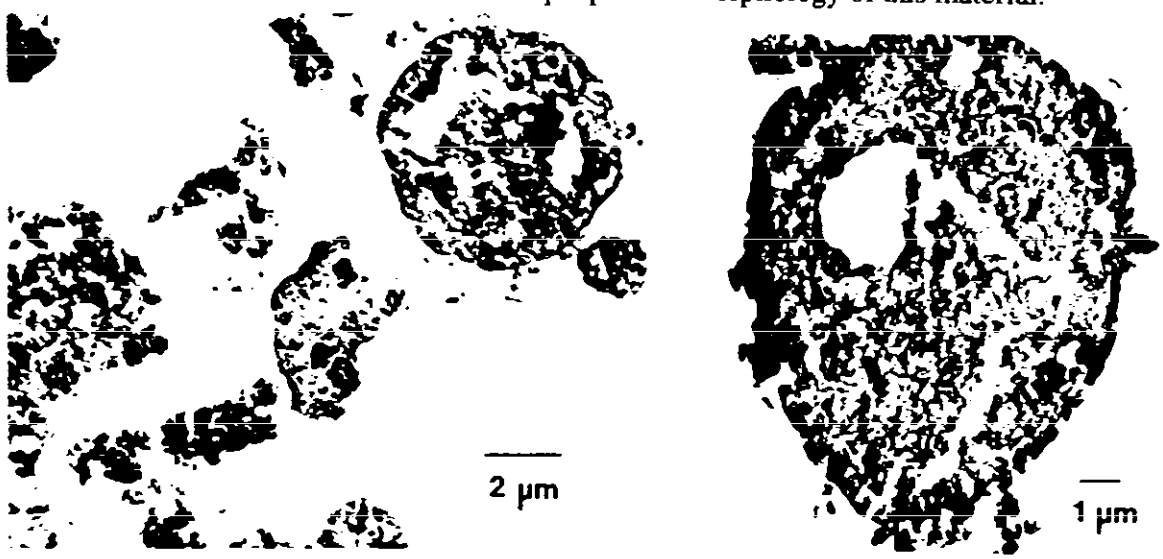

Fig. II.1 Analytical transmission electron microscopy images of thin sections of the Silo 3 material. The images illustrate the variety of particle morphologies. These particle morphologies have important consequences with regard to diffraction studies with both X-rays and electrons. In (a) a series of particles can be seen, including Mo-vanadates, As-bearing phosphates, other forms of phosphates, and quartz. These particles are described in more detail later. In (b) the material consisted of iron phosphate and silicates, as well as a few tin oxide particles.

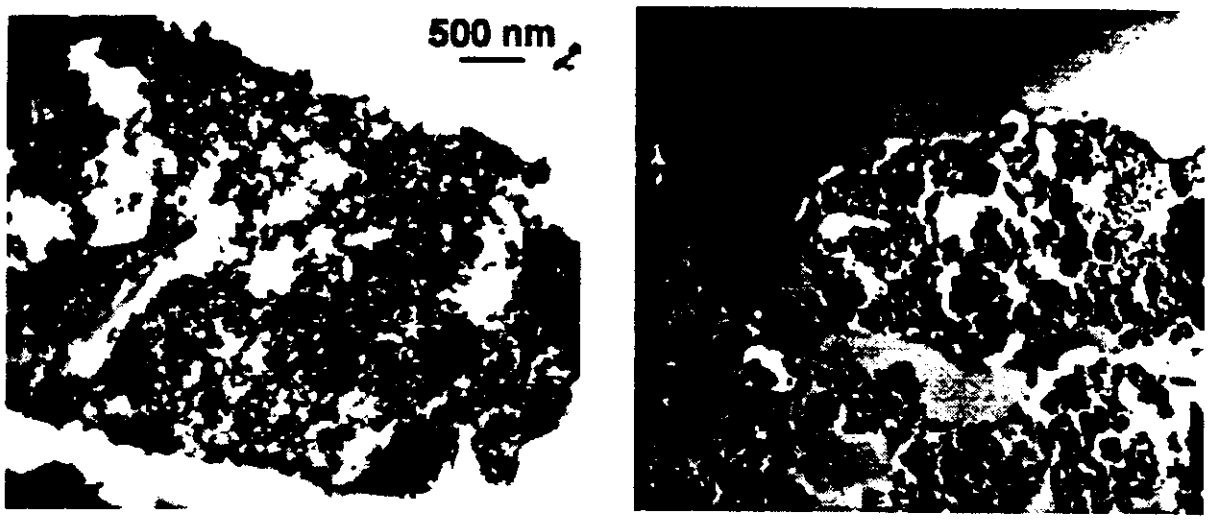

Fig. II.1 (cont.) In (c) the major component is an iron silicate and in (d) a mixture of silicate and magnesium phosphates were present. These particles represent many of the major phases in the Silo 3 material.

ANALYTICAL TRANSMISSION ELECTRON MICROSCOPY RESULTS

The major phases were determined to be quartz, Mg- and Fe- phosphates, iron oxides, and calcium sulfate. The actinide were present as nanocrystalline particles of silicates, oxides, and phosphates. The results from the AEM study are broken into the major categories of phosphates, silicates, oxides, and sulfates.

Phosphates

The major phosphate phase in the Silo 3 material was a magnesium phosphate containing small amounts of calcium, manganese, and iron. Examples of these phases can be in Figures II.1-II.5. The composition of these phases varied. The major cations appeared to be iron and magnesium with minor amounts of calcium, or transition metals. Based on electron energy loss spectroscopy analysis, ammonium ion may also be present. Most of the nitrogen in the Silo 3 material may be present in this form. Phosphate was also often replaced by small amounts of arsenate. Iron phosphates were also dominant in the Silo 3 material. Arsenic was often found, as arsenate, in the phosphorus-bearing material, along with small amounts of uranium on occasions

Table II.1. Measured electron diffraction parameters from a rare-earth-bearing phosphate phase compared to literature x-ray diffraction parameters of a monazite-type phase.

d_{obs} (nm)[1] REE Phase	d_{lit} (nm) brabantite[2]
0.664	possible (100 reflection)

0.312	0.312
0.307	0.306
0.262	0.258
0.166	0.167

Errors in d-spacings are ±5%. It has been assumed that the Nd, La-analogue would be structurally similar to the known Th-bearing phase; although, many reflections in the experimental pattern were missing, this is a reasonable match.
[2]Unit cell parameters for brabantite of the monazite group are **a** =0.671 nm, **b** = 0.692 nm, and **c** = 0.642 nm and β= 103.75 [JCPDS 31-311].

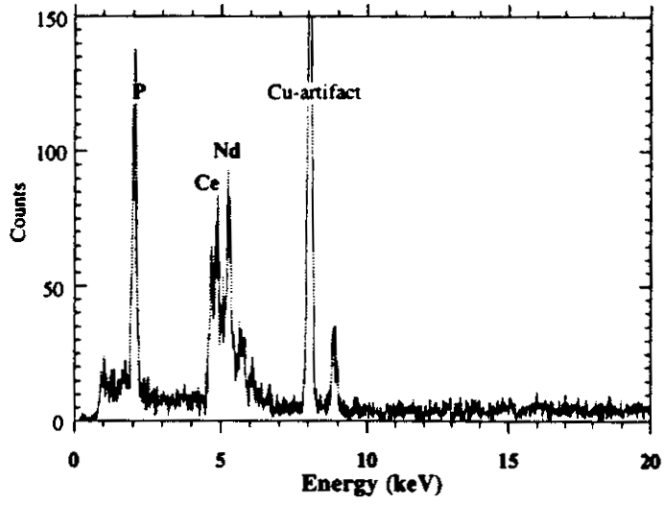

Fig. II.2 X-ray energy dispersive analysis of a rare earth-bearing phase, compositionally related to monazite-type phase. These types of particles are shown in Fig. I.4, which is a SEM/BSE image. The proposed formula based on the EDS analysis is $CeNd(PO_4)_2$.

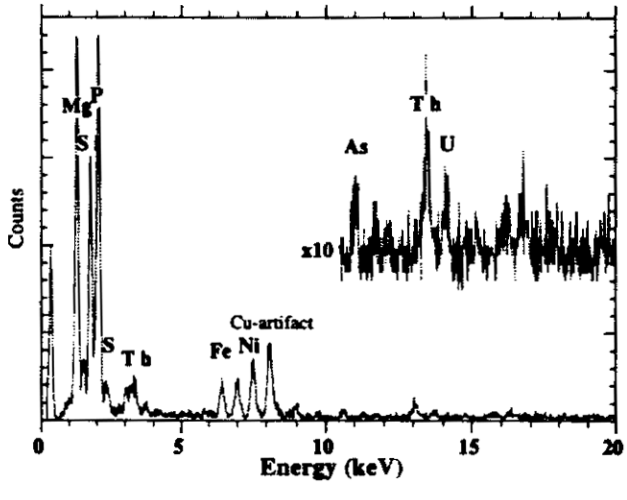

Fig. II.3 X-ray energy dispersive analysis of a thorium-bearing phase, possibly $Th_{0.1}Mg(PO_4)(SiO_4)_{0.8}$. The phase may be a member of the alunite group. At least two different phases are present in this spectrum, including Mg-phosphate and an iron silicate.

Table II.2. Measured electron diffraction parameters from a calcium and magnesium-bearing phosphate phase compared to literature x-ray diffraction parameters of fairfieldite $Ca_2(Mg,Fe)(PO_4)_2 \cdot 2H_2O$.

d_{obs} (nm)[1] Ca-Mg-PO_4 Phase	d_{lit} (nm) Fairfieldite[2]
1.1801	
0.6744	0.640
0.434	0.433
0.368	0.360
0.343	0.348
0.334	0.334
0.308	0.303
0.288	0.286
0.272	0.269
0.248	0.246
0.225	0.224
0.213	0.213

[1]Errors in d-spacings are ±5%.
[2]Unit cell parameters for triclinic fairfieldite are **a** = 0.578 nm, **b** = 0.657 nm, and **c** = 0.548 nm, α= 102°, β= 108.7°, and γ= 90.08° [JCPDS 10-390].

The electron diffraction data were compared to the most closely related mineral phases found. As the type of cation in a particular phase may vary, the compositions of the matching phase may not always match that of the observed phase. In the case of fairfieldite, a calcium-bearing variety has been matched to the observed phase. It is entirely possible that the calcium ions may be replaced by magnesium ions yielding a phase which is structurally (X-ray or electron diffraction) identical to the mineral phase reported in the literature.

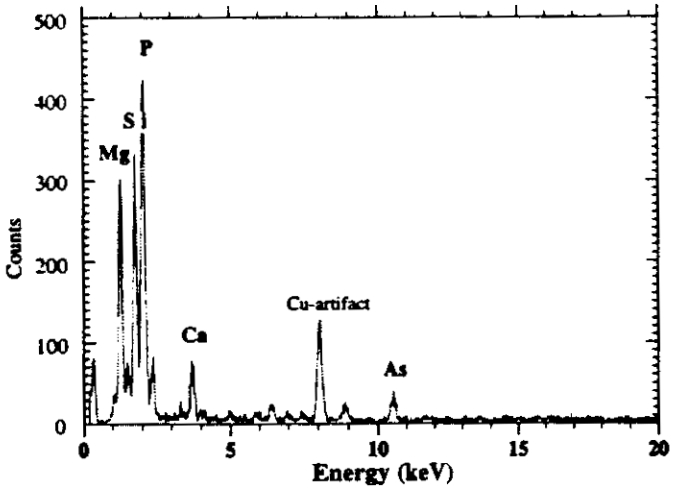

Fig. II.4 X-ray energy dispersive analysis of a magnesium arsenophosphate phase, possibly $MgCa_{0.2}(SiO_4)_{0.8}(PO_4)(AsO_4)_{0.3}$. Silicon dixoide and calcium sulfate are also present. In this example, the As concentration is fairly high, around 5 wt%; however, in most other cases, the concentration was barely detectable (i.e. <0.5 wt%).

Table II.3. Measured electron diffraction parameters from an iron-bearing phosphate phase compared to literature x-ray diffraction parameters.

d_{obs} (nm)[1]	d_{lit} (nm)
$FePO_4$ Phase	chalcosiderite [2]
0.215	0.214
0.188	0.187
0.180	
0.161	

Table II.4. Measured electron diffraction parameters from an iron-bearing phosphate phase compared to literature x-ray diffraction parameters.

d_{obs} (nm)[1]	d_{lit} (nm)
$FePO_4$ Phase	chalcosiderite [2]
1.136	1.28
0.771	0.768
0.434	
0.383	0.377
0.315	
0.302	0.302
0.271	0.271
0.256	0.259
0.233	0.231
0.221	
0.218	0.214
0.196	0.196
0.186	0.187
0.153	0.154

[1]Errors in d-spacings are ±5%.
[2]chalcosiderite, ideally $CuFe_6(PO_4)_4(OH)_8 \cdot 4H_2O$ is a triclinic phase of the turquoise group [JCPDS 8-127]. Matches well compositionally in terms of the Fe to P ratio. Copper can be difficult to detect with the EDS system as it appears as an artifact during all analyses; however, the K to L ratio for Cu is a good indication for the presence of Cu in a phase. The match with the electron diffraction is also very good.

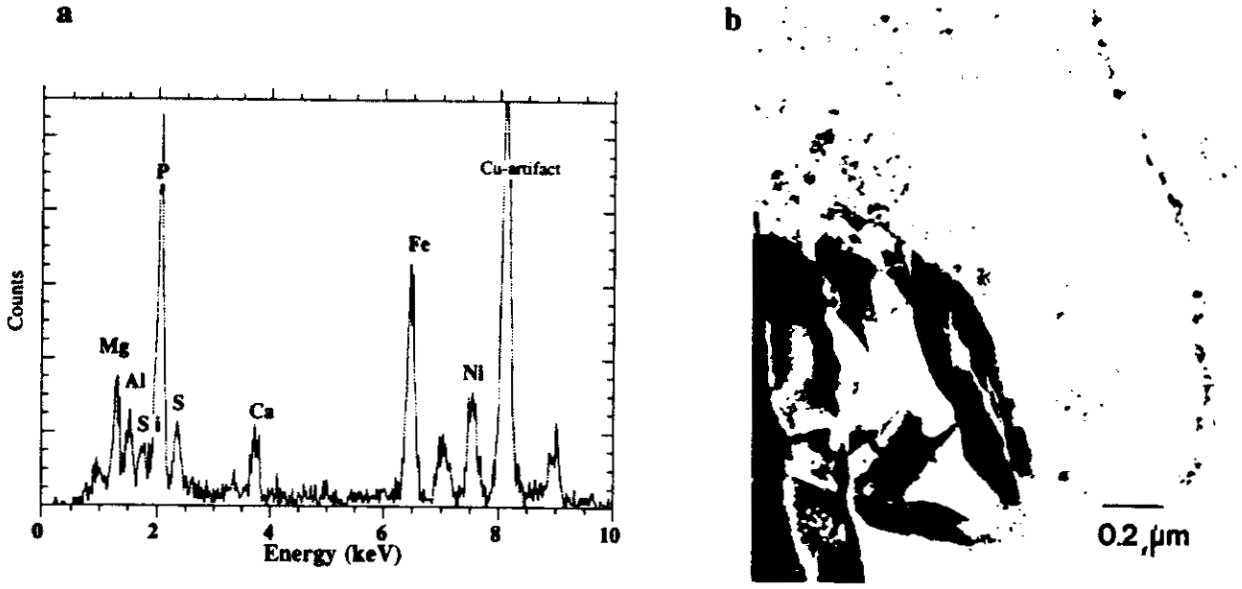

Fig. II.5 (a) X-ray energy dispersive analysis of an iron phosphate, EDS analysis suggest the composition is $FeNi_{0.5}(PO_4)_2$ phase, possibly related to vivanite $(Fe_2Ni)(PO_4)_2 \cdot H_2O$). This phase also appears to incorporate the Ni present in the sample. After the magnesium-bearing variety, this was the most common form of phosphate in the sample. Some crystals were cryptocrystalline and others existed as well-formed crystals. The AEM image in (c) show a central region containing iron silicate with a magnesium phosphate rim.

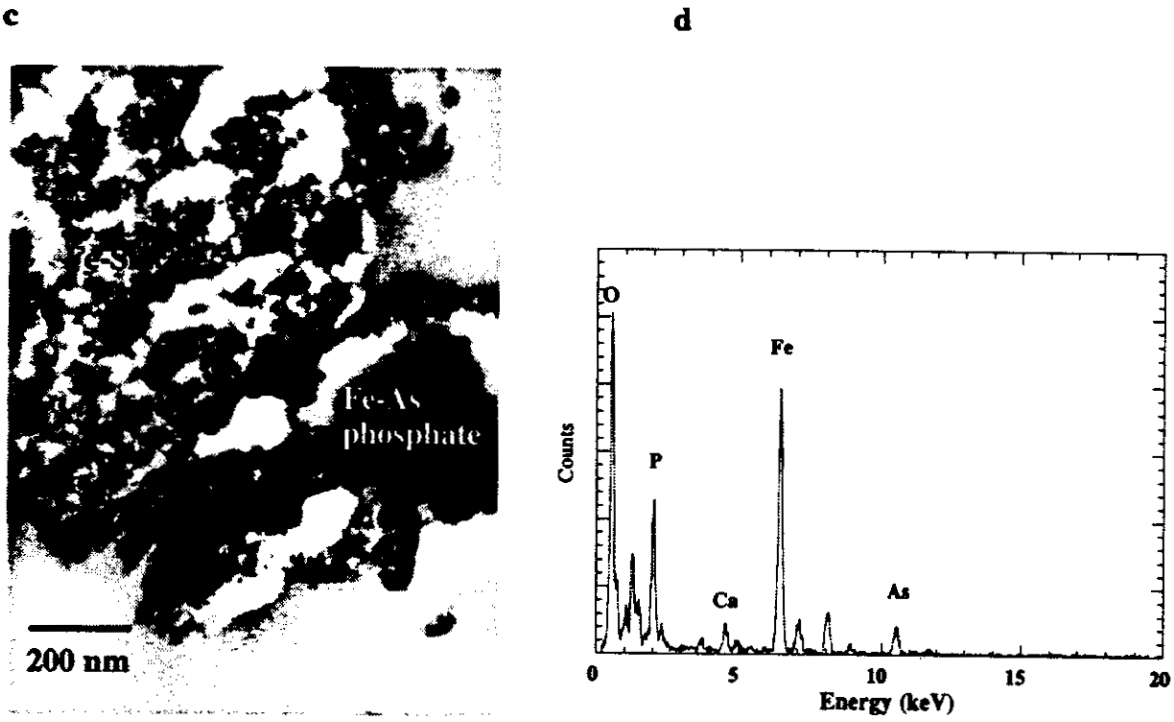

Fig. II.5 (cont..) (c) Shows a region containing iron and arsenic with a iron silicate matrix. (d) The EDS analysis of the iron phosphate phase indicates a significant amount of arsenic.

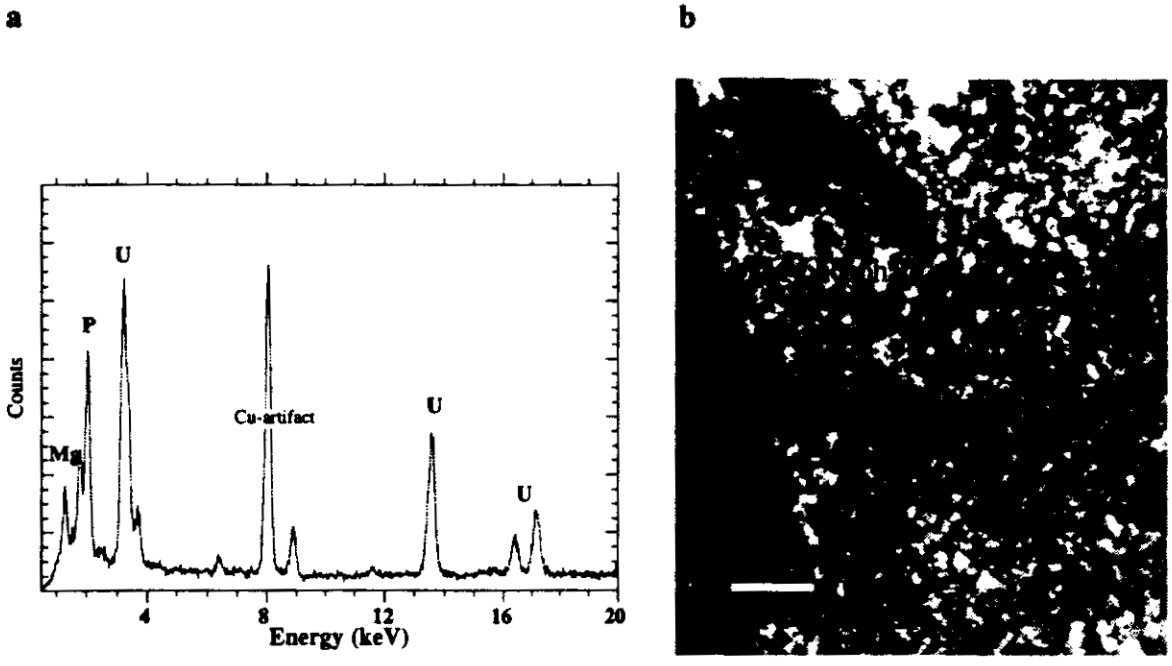

Fig. II.6 (a) X-ray energy dispersive analysis of a magnesium uranium phosphate phase, possibly saleeite ($Mg(UO_2)_2(PO_4)_2 \cdot 9H_2O$). The TEM image (b) shows the disposition of these types of phases within a large matrix of phosphate.

Silicates

Silicates included calcium and potassium aluminosilicates, as well as a number of actinide silicates, including possibly ursilite. The potassium aluminosilicate was clearly related to illite-type minerals (i.e. mica and biotite) and the Na- Ca-aluminosilicate is possibly a zeolite. Both these phases are known to precipitate within reasonable time periods from silica-saturated solutions at room temperatures; however, many of the other silicates appeared to be high temperature phases, including the pyroxenoid phase, wollastonite and quartz (SiO_2). In Table. II.5, electron diffraction data from the calcium silicate is shown. The major silicate was identified as quartz (see Table II.6) and most of the silicon present is assumed to be present as quartz.

Both phosphate, silicate and carbonate groups may undergo isomorphic substitution in many minerals for each other to a limited extent. This evident in the Silo 3 material, where some phases appear to combinations of silicon and phosphorus. This is considered to be the most likely form of carbon in the material.

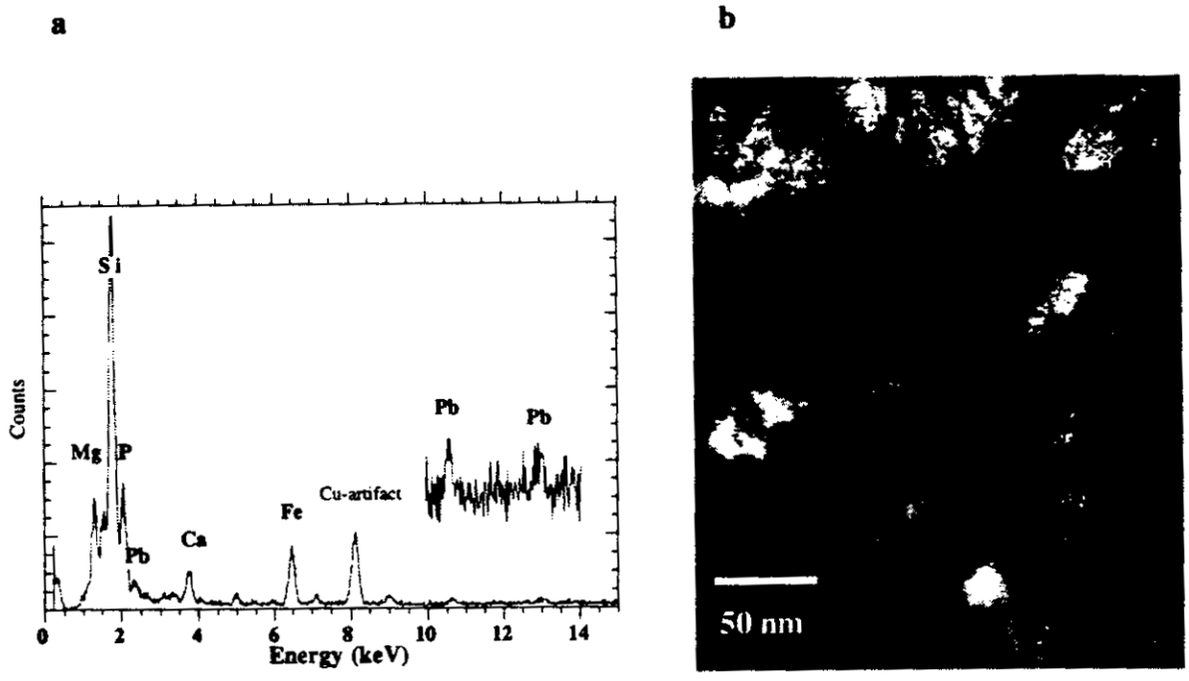

Fig. II.7 (a) X-ray energy dispersive analysis of a silicate from fibrous region of sample shown in (b). Although the major form of silica was quartz, a number of other forms were also present. The occurrence of these forms makes interpretation of the distribution of compounds in the sample difficult. In this case, the phase also contained a small amount of lead, < 0.5 wt%.

Table II.5. Measured electron diffraction parameters from a calcium silicate phase compared to literature x-ray diffraction parameters.

d_{obs} (nm)[1] Ca-SiO_x Phase	d_{lit} (nm) Wollastonite[2]
0.487	0.448
0.484	
0.402	0.406
0.363	0.351
0.328	0.331
0.245	0.244
0.227	0.227
0.159	0.160
0.157	0.157
0.150	0.151

[1]Errors in d-spacings are ±5%.
[2]Wollastonite, ideally $CaSiO_3$, appears in monoclinic and triclinic forms. The mineral belongs to the pyoxenoid group. The match with the collected electron diffraction data is reasonable.

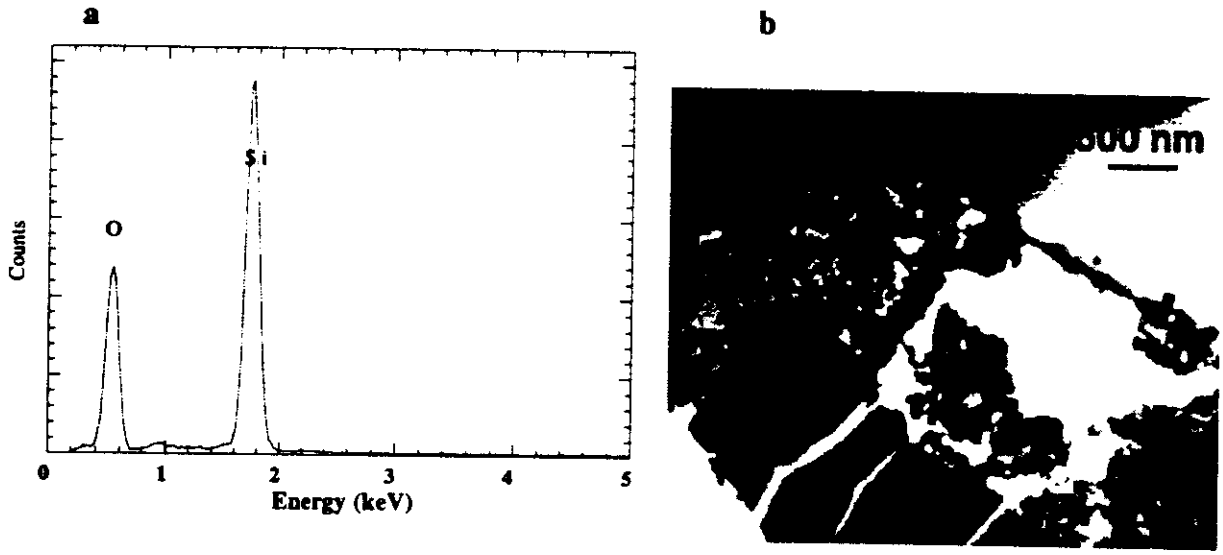

Fig. II.8 (a) X-ray analysis of quartz from Silo 3 material and (b) TEM image of quartz particle with a surface of amorphous material coating the particle.

Table II.6. Measured electron diffraction parameters from a silicate phase compared to literature x-ray diffraction parameters.

d_{obs} (nm)[1] SiO_x Phase	d_{lit} (nm) quartz [2]
0.389	
0.2604	
0.214	0.213

[1]Errors in d-spacings are ±5%.
[2] quartz (SiO_2) is hexagonal with **a** = 0.491 nm and **c** = 0.540 nm

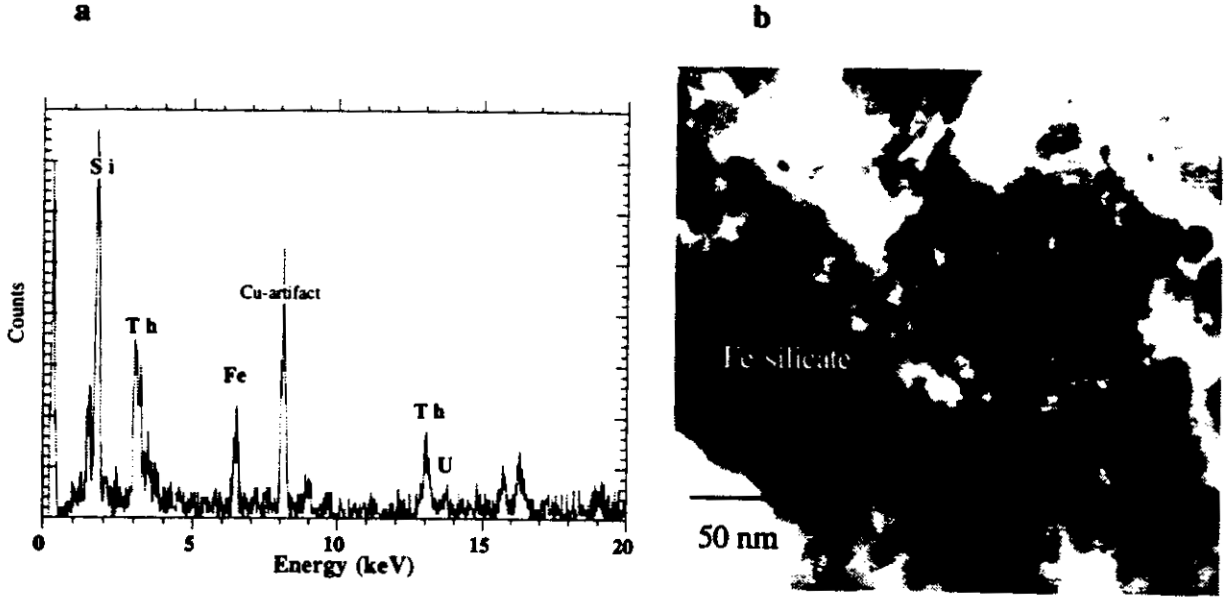

Fig. II.9 (a) X-ray energy dispersive analysis of a thorium iron silicate, estimated to be $ThFe_{0.5}Si_2O_8$. A small amount of uranium is also present in this phase. (b) TEM image showing the presence of colloidal-sized thoria particles.

The electron diffraction analysis in Table II.7 shows data from a sodium-bearing phase. These phases are assumed to be the most common form for sodium in the Silo 3 material.

Table II.7. Measured electron diffraction parameters from a sodium calcium alumino-silicate phase compared to literature x-ray diffraction parameters.

d_{obs} (nm)[1] K-$AlSiO_x$ Phase	d_{lit} (nm) illite[2]
0.458	
0.455	0.452 (020)
0.264	0.260
0.263	
0.172	0.172

[1] ±5% error

[2] illite ($KAl_2(Si_3AlO_{10})(OH)_2$) is monoclinic with **a** = 0.52 nm, **b**= 0.9 nm, **c** = 1.001 nm, and β = 90°.

The electron diffraction analysis in Table II.7 was from a single crystal pattern. The pattern was hexagonal which is supportive a <001> zone axis of illite. This phase may be the main potassium-bearing phase.

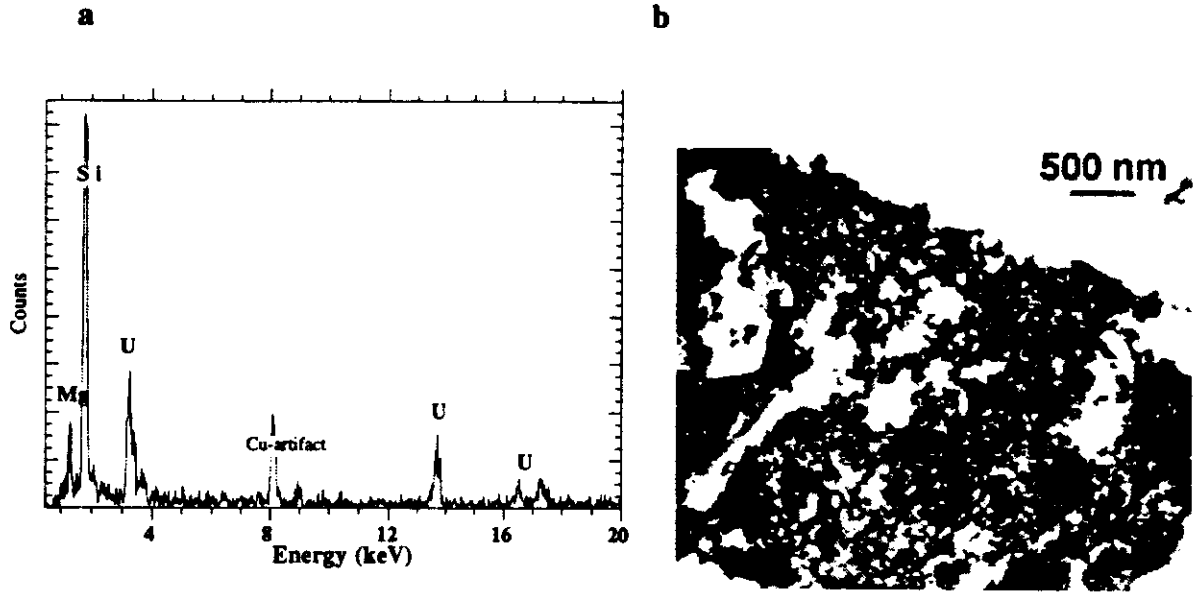

Fig. II.10 (a) X-ray energy dispersive analysis of a magnesium uranyl silicate phase, possibly ursilite, ideally $Mg_2(UO_2)_2(Si_5O_{16})\cdot 9H_2O$. (b) Transmission electron microscopy image of iron silicate phase. This phase exhibits a cryptocrystalline structure.

Oxides and other phases

Iron oxides were commonly observed in the Silo 3 material (see Fig. II.11 and Table II.8). The morphology of these particles varied from cryptocrystalline to larger particles. The uranium is probably sorbed to the surface of the hematite. Hematite is the most commonly found form of iron oxide under most pH-Eh conditions. The presence of vanadium and molybdenum has resulted in the formation of vanadates and molybdates (see Fig. II.12). These minerals were often enriched in actinides.

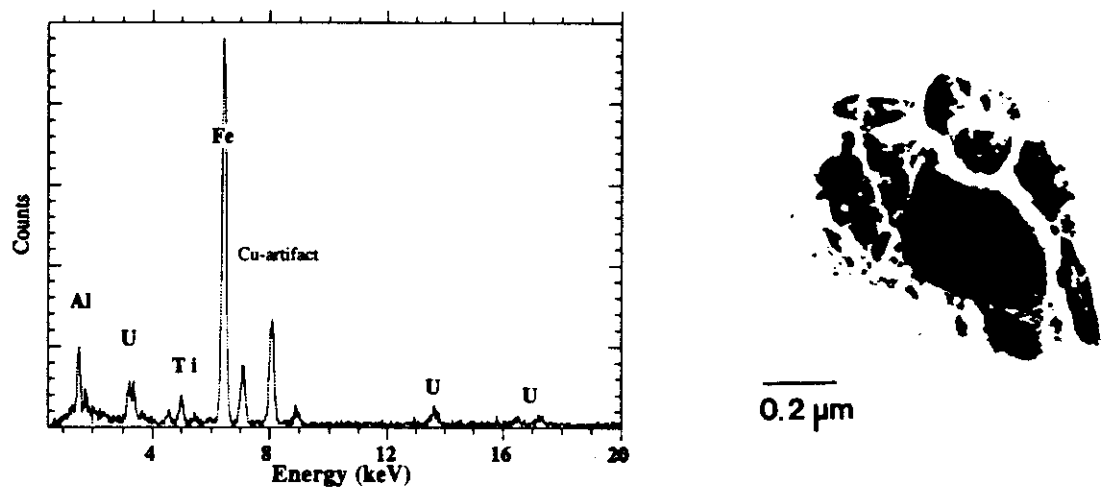

Fig. II.11 (a) X-ray energy dispersive analysis of an iron phase containing a small amount of uranium. There are large amounts of iron in the sample. (b) Transmission electron microscopy image of an iron oxide phase.

Table II.8. Measured electron diffraction parameters from an iron oxide phase compared to literature x-ray diffraction parameters.

d_{obs} (nm)[1] Fe_2O_3 Phase	d_{lit} (nm) hematite[2]	d_{lit} (nm) goethite[3]
1.147		
0.434		
0.422		0.418
0.393		
0.368	0.368	
0.328		0.338

d_{obs} (nm)[1]	d_{lit} (nm) hematite[2]	d_{lit} (nm) goethite[3]
0.351	0.368	
0.243	0.252	0.245
0.215	0.221	0.219
0.197	0.208	0.192
0.169	0.169	0.169

[1]Errors in d-spacings are ±5%.
[2]Hematite (Fe_2O_3) is hexagonal with **a** = 0.5036 nm and **c** = 1.3749 nm [JCPDS 24-72].
[3]Goethite (FeO(OH)) is orthorhombic with **a** = 0.4608 nm, b = 0.9956 nm, and c = 0.3021 nm [JCPDS 29-713]

Fig. II.12 (a) X-ray energy dispersive analysis a iron vanadium molybdate phase (possibly $Fe(VO_4)(MoO_4)_2$) with the iron from a separate phase.

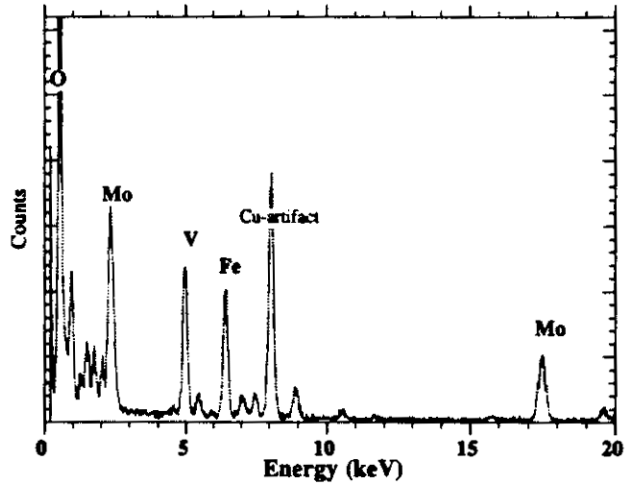

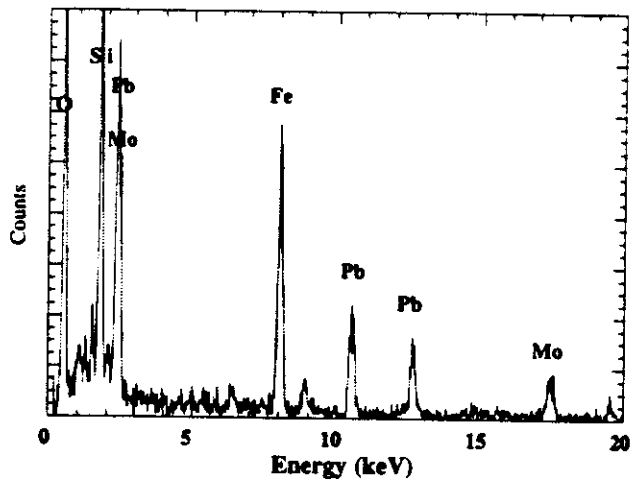

Fig. II.12 (cont..) (b) and an iron lead molybdate phase. (c) Transmission electron microscope image of iron vanadate. The electron diffraction analysis of this phase is shown in Table II.9.

Table II.9. Measured electron diffraction parameters from an iron-vanadate phase compared to literature x-ray diffraction parameters.

d_{obs} (nm)[1] FeTi(VO_4)Phase	d_{lit} (nm) davidite[2]
0.699	0.686
0.343	0.342
0.256	0.259
0.180	0.180
0.177	0.178
0.173	0.171, 0.174
0.163	0.160
0.156	0.155

[1] ±5% error in measurement.
[2] Davidite $(Fe,U)(Ti,V)_3(O,OH)_7$ is hexagonal with **a** = 1.037 nm and **c** = 2.087 nm.

The analysis of many of the phases found during the TEM examination showed very complex compositions. It was not always possible to provide a unique identification for some of these phases.

The composition analysis of an iron and lead bearing phase indicated roughly equal amounts of S and P in the phase. Compositionally this phase matches well with corkite, alunite group. The electron diffraction from the phase is shown in Table II.10. This phase illustrates the

point concerning isomorphic substitution of some structural groups in these minerals. It also demonstrates the difficulty in determining the proportions of phases in the Silo 3 material.

Table II.10. Measured electron diffraction parameters from an iron-lead sulfate-phosphate phase compared to literature x-ray diffraction parameters.

d_{obs} (nm)[1] $Fe(PO_4)(SO_4)$ Phase	d_{lit} (nm) corkite[2]
0.355	0.361
0.342	0.347
0.248	0.251
0.244	0.234
0.196	0.196
0.153	0.152

[1] ±5% error
[2] Corkite $PbFe_3(PO_4)(SO_4)(OH)_6$ is hexagonal with **a** = 0.722 nm and **c** = 1.666 nm

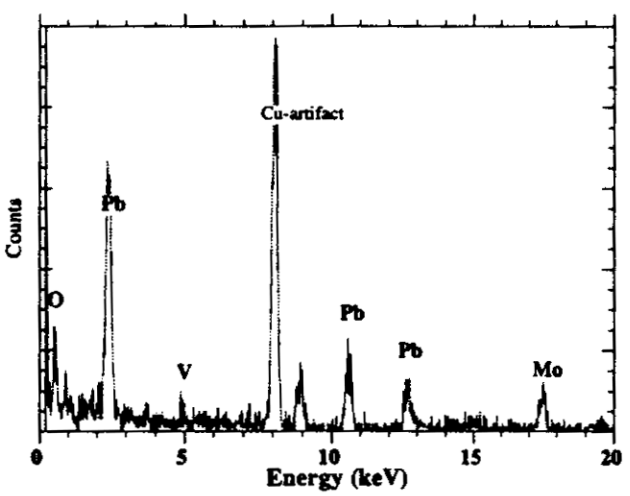

Fig. II.13 X-ray energy dispersive analysis of a lead oxide (PbO_2) phase, possibly plattnerite (rutile group). Lead particles were also observed in the SEM images and evidence of trace peaks from these phases were visible in the XRD scans. The heavy element oxides, which are present in minor amounts, will be strong scatters of the X-ray beam. This makes them more visible than many other more dominant (in terms of volume) phases. The Mo-V peaks may be from a separate phase, as this composition was observed elsewhere (see above).

Table II.11. Measured electron diffraction parameters from an aluminum oxide phase compared to literature x-ray diffraction parameters.

d_{obs} (nm)[1] Al_2O_3 Phase	d_{lit} (nm) corrundum[2]
0.166	0.174, 0.160
0.144	0.140
0.135	0.137, 0.134

[1] ±5% error
[2] corrundum (Al_2O_3) is hexagonal with **a** = 0.4758 nm and **c** = 1.2991 nm

Sulfur-bearing phases

Sulfur is present in the Silo 3 material at levels which will certainly cause problems during vitrification. Both calcium- and iron- sulfur bearing compounds were both observed in the Silo 3 material.

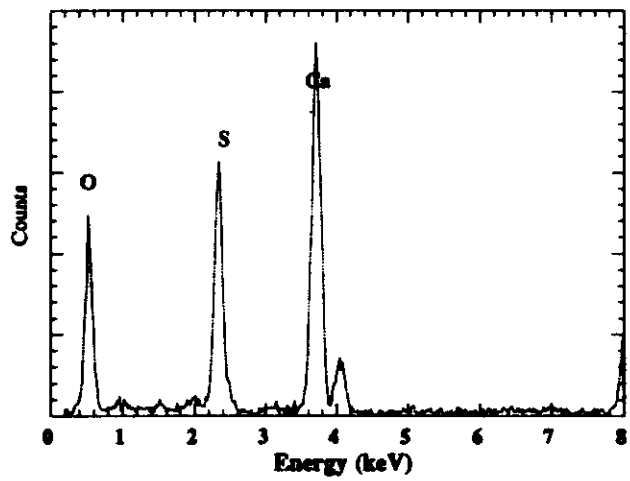

Fig. II.14 (a) X-ray energy dispersive analysis of the major calcium sulfate phase from the Silo 3 material. The composition of this phase suggests a Ca:S ratio of about 3:2.

The information on the iron-bearing phase has not been obtained.

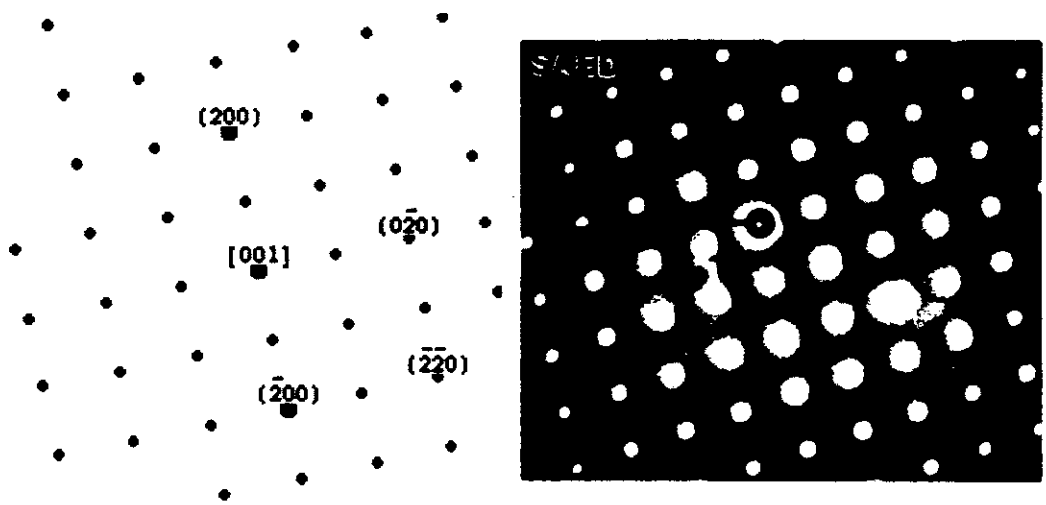

Fig. II.14 (b) Computer simulated pattern of calcium sulfate (anhydrite) and (b) an experimentally obtained diffraction pattern from a particle in the Silo 3 material.

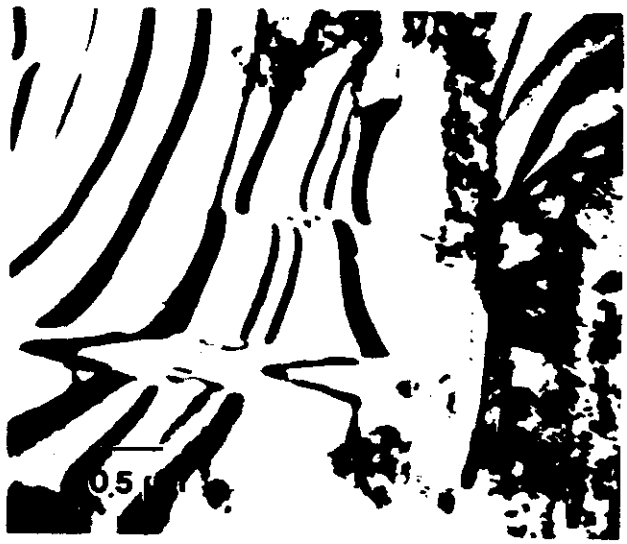

Fig. II.15 Transmission electron microscopy image of euhedral crystal of calcium phase. These types of crystals diffraction well and therefore are more visible in the XRD scan than the cryptocrystalline phases, even if these phases are more dominant.

There was some difficulty in identifying the major sulfur-bearing phase. Many of the reflections found suggested that the phase may be a sulfite. No match could be made with the most obvious S-bearing phase, gypsum. The match with orschallite, which is a mixed sulfite-sulfate mineral was very good (see Table II.12) and it was also possible to match the zone axis patterns obtained; however, this phase has a very large c- axis spacing which could not be reconciled with the electron diffraction patterns. The XRD data was unable to distinguish these differences although it clearly did not show any large d-spacings. Oddly enough, the EDS indicated that the Ca:S ratio was slightly greater than one. This may suggest the presence of undetected species such as carbonate. During the SEM and AEM studies, no phases were identified which indicated the source of the carbon. The sulfur-bearing phases did match anhydrite-type phases reasonably well, but not as good as orschallite. The zone axis patterns supported a smaller unit cell, which orschallite does not possess and this was the key piece of information supporting the assignment of anhydrite. There are several varieties of anhydrite depending on the degree of hydration, with eventually gypsum being formed. The XRD results could be fitted with several S-bearing compounds including, orschallite and anhydrite.

Table II.12. Measured electron diffraction parameters from the calcium sulfur-bearing compared to literature x-ray diffraction parameters.

d_{hkl} (nm)[1] Phase	d_{hkl} (nm) anhydrite[2]	d_{hkl} (nm) orschallite[3]
0.4842		0.487
0.4821		
0.4662		0.463
0.3702	0.387	0.367
0.3631	0.350	0.363
0.3291	0.312	0.328
0.3284		
0.3228		0.311
0.2317	0.233	0.235
0.173	0.175	0.176
0.163	0.165	0.164
0.156	0.156	0.159

[1] ±5% error
[2] anhydrite ($CaSO_4$) is orthorhombic with a = 0.6238 nm, b = 0.6996 nm, and c = 0.6991 nm
[3] orschallite ($Ca_3(SO_3)_2SO_4 \cdot 12H_2O$) is hexagonal with a = 1.135 nm and c = 2.832 nm

Nitrogen-bearing compounds

Nitrogen is can be detected with X-ray methods; however, this not a reliable method for low concentrations. Parallel electron energy-loss spectrometry (EELS) is more effective for detecting this element. The results from XRD suggested the presence of sodium nitrate (nitratite), although this was not supported by any other technique. During the analysis of the samples, phases were not found which had an obvious deficiency of species. Nitrogen was observed in some of the phosphate phases with EELS (see Fig. II.16) which suggests it may be present as an ammonium ion in the phase.

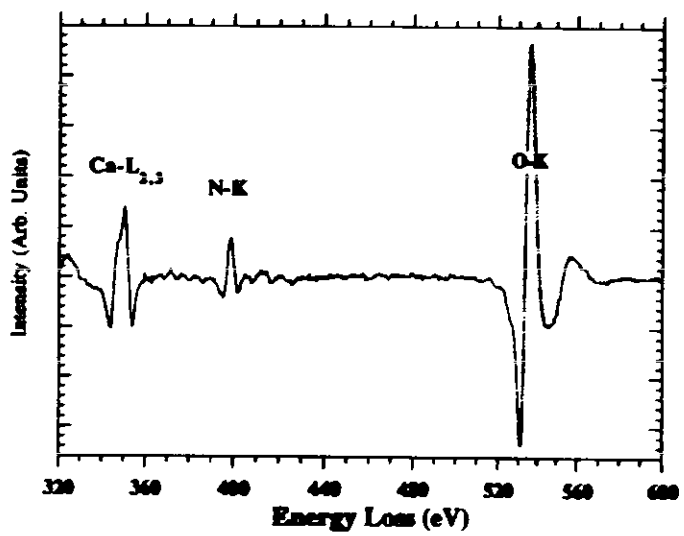

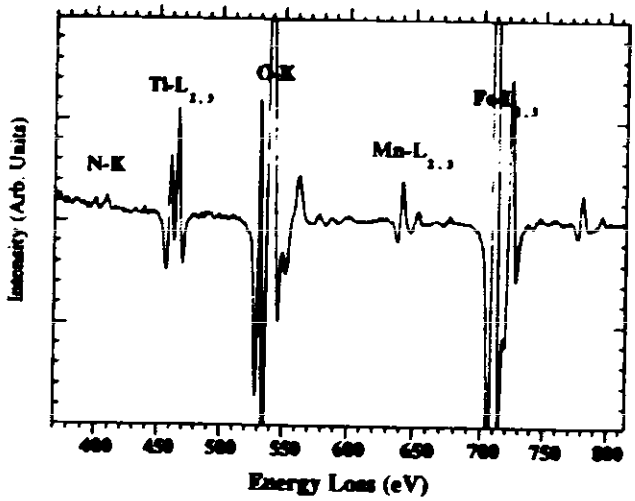

Fig. II.16 (a) Electron energy-loss spectrum of phase showing the presence of nitrogen in the phase. This was a calcium-bearing phase. (b) iron-bearing phase which also appears to contain some nitrogen.

In order to answer the sulfate/sulfite question, further analyses were made with diffraction and spectroscopic methods. The data were compared to bassanite, orschallite, hannebachite, anhydrite, and gypsum which are representative of important calcium sulfate and sulfite minerals. The XRD data matched with bassanite, orschallite, and anhydrite. After some lengthy investigations with TEM and XRD, it is apparent that the this sulfur-bearing phase is a variety of anhydrite. The iron sulfur compound is also present as a sulfate.

III. X-RAY DIFFRACTION ANALYSIS

BACKGROUND

The object of the X-ray diffraction (XRD) analysis was to determine the major phases in the sample. X-ray diffraction can be applied to "bulk" samples whereas electron diffraction is for ultra-thin samples. The advantage of the technique is that it provides a rapid analysis of all phases in the sample and we can use it to provide some estimate of the amounts of each phase. The disadvantage of this technique when used with heterogeneous samples is that it is difficult to determine which reflection corresponds to which phase. The powder diffraction method used also provides no composition information. The microscopy studies indicate that many of the phases will be poor scatters of X-rays, owing to their cryptocrystalline or amorphous nature. The well-formed (euhedral) particles, particularly the calcium sulfate and quartz particles, provided the most intense scattering, whereas, the cryptocrystalline phosphates diffraction poorly. This means that we can not use the intensity of a diffraction peak as an absolute indication of that phases level in the sample. The XRD also has problems with amorphous materials, as these are not good scatters of the X-ray beam. The electron microscopes have an advantage in this respect.

The XRD scan of the Silo 3 material was provided by P. Johnson of the ANL-analytical chemistry laboratory (ACL).

DOCUMENTATION

Complete records of the experimental procedures followed in the examination of the Silo 3 material with X-ray diffraction are recorded in scientific notebook #1160. The raw data is attached to the end of this report.

SYSTEM DESCRIPTION

The XRD analysis was carried out with a Rigaku XRD instrument. Phases were identified by comparing the known diffraction analyses reported in the literature using compositional information from the SEM and wet chemical analyses. The data were refined as far as possible using the TEM data.

SAMPLE PREPARATION

Samples for X-ray diffraction were prepared by mounting a portion of the powder on holding tape.

X-RAY DIFFRACTION RESULTS

The XRD results were interpreted with the help of the TEM for the individual phases' composition and structure and with the SEM results for the overall composition material balance.

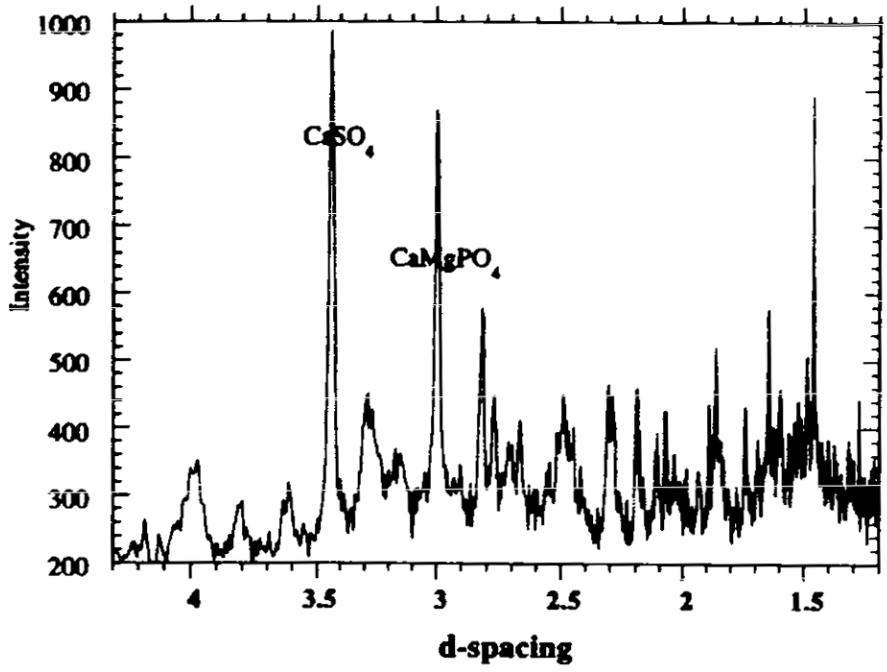

Fig. III.1 X-ray diffraction analysis of Silo 3 material showing prominent peaks for fairfieldite ($Ca_2(Mn,Fe)(PO_4)_2 \cdot 2H_2O$), chalcosiderite ($CuFe_6(PO_4)_4(OH)_8 \cdot 4H_2O$), anhydrite $Ca(SO_4)$, and quartz (SiO_2).

Table. III.1 Listing of major reflections from XRD analysis of Silo 3 material

d-spacings	Possible assignment	d-spacings	Possible assignment
3.9757	fairfieldite	2.1040	*chalcosiderite*, anhydrite
3.6151	*chalcosiderite*, fairfieldite,	2.0692	corundum
3.4373	quartz, corundum, anhydrite, *chalcosiderite*	1.8825	fairfieldite, nitratite
3.2827	faifieldite	1.8540	quartz, *chalcosiderite*, fairfieldite, *hematite*
2.9947	fairfieldite, bassanite, *chalcosiderite*, nitratite	1.7328	corundum
2.8119	anhydrite, nitratite	1.6837	fairfieldite, *hematite*
2.7655	*hematite*	1.6370	
2.6613	fairfieldite,	1.5912	corundum, quartz,
2.4857	*hematite*, quartz, corundum, stanfieldite	1.4816	*hematite, chalcosiderite*
2.3044	fairfieldite, anhydrite, nitratite	1.4535	*hematite*
2.1871	corundum, anhydrite	1.2711	

The matches for phases are generally poor owing to the microcrystalline nature of most of the compounds in the sample and the rapid XRD scan. Diffraction intensities for the iron oxide, calcium sulfite, and silicon dioxide phases were expected to be greatest, as these particles exist as micron-sized euhedral crystals. The major other phases, magnesium phosphate and iron phosphate, were cryptocrystalline and will not diffract well.

IV. WET CHEMICAL ANALYSIS

BACKGROUND

The object of the wet chemical analysis was to determine the composition of the sample and to compare the results to those obtained by other laboratories.

DOCUMENTATION

Complete records of the experimental procedures followed in the examination of the Silo 3 material by ICP-MS are recorded in scientific notebook #1160.

SYSTEM DESCRIPTION

The ICP-MS analyses in this study are conducted on a Fisons VG PlasmaQuad II+ series ICP-MS instrument (FI Elemental Analysis, Winsford, Cheshire, UK) modified for containment within a fume hood. The plasma torch and interface, with sampler and skimmer cones, are installed inside the hood, while the mass spectrometer and associated electronics are outside the hood. This instrument is equipped with a V-groove DeGalan nebulizer and a Scott double-pass spray chamber cooled with a circulating ethylene glycol/water refrigeration unit set to 2.5°C (model RTE-110A, Neslab, Portsmouth, NH). Sample uptake is controlled with a peristaltic pump (Minipuls 3, Gilson Medical Electronics, Middleton, WI). The detector is a Model 4870 channeltron electron multiplier (Galileo Electro-Optics, Sturbridge, MA). System control, data acquisition, and analysis are performed using PQ Vision version 4.1.2 (FI Elemental Analysis, Winsford, Cheshire, UK).

CALIBRATION

Mass calibration and instrumental mass response were corrected by analyzing a solution containing 10 mg/L of Be, Mg, Co, Ni, In, Ce, Pb, Bi, and U on each day of analysis. Temporal stability of the instrument is also checked weekly with this solution. Unknown samples are spiked with an internal standard so that they contain 50 µg/L of Be, Sc, Y, In, Tb, and Bi. A mass spectrum is acquired by scanning the quadrupole from 5.5 to 249.5 amu with a 320 µs dwell time. Mass spectra are usually acquired with two 60-s acquisitions. Concentrations were calculated

using multi-elemental standards. Transuranic radionuclide concentrations were calculated from blank-subtracted spectra, with ^{209}Bi as an internal standard.

SAMPLE PREPARATION

A 200 mg sample was dissolved by boiling with $HF+HNO_3+HCl$ in an open Teflon beaker on a hot plate and taken to dryness. The sample was fumed with $HClO_4$ to ensure complete dissolution of rare earth and transuranic elements, dissolved in 1 mL HCl, and diluted to 100 mL. This procedure was repeated using a 500 mg sample.

ICP-MS RESULTS

Table IV.1 ICP-MS Results from the dissolution of the Silo 3 Material

Element	soln.1	solid 1	soln.2	solid 2	average [ppm]	σ[ppm]
Na	**157200**	**3.7 x 10^4**	**197400**	**3.9 x 10^4**	**3.8 x 10^4**	**9.2 x 10^2**
Mg	**255100**	**6.1 x 10^4**	**334900**	**6.6 x 10^4**	**6.3 x 10^4**	**3.5 x 10^3**
Al	**109200**	**2.6 x 10^4**	**149900**	**2.9 x 10^4**	**2.8 x 10^4**	**2.4 x 10^3**
Si			350000	6.9 x 10^4	6.9 x 10^4	-
K	39870	9.5 x 10^3	44940	8.8 x 10^3	9.2 x 10^3	4.8 x 10^2
Ca	**125400**	**3.0 x 10^4**	**100700**	**2.0 x 10^4**	**2.5 x 10^4**	**7.1 x 10^3**
V	8958	2.1 x 10^3	11470	2.2 x 10^3	2.2 x 10^3	8.3 x 10^1
Cr	792	1.9 x 10^2	2237	4.4 x 10^2	3.1 x 10^2	1.8 x 10^2
Mn	20330	4.8 x 10^3	25920	5.1 x 10^3	5.0 x 10^3	1.7 x 10^2
Fe	**256600**	**6.1 x 10^4**	**267100**	**5.2 x 10^4**	**5.7 x 10^4**	**6.1 x 10^3**
Co	11370	2.7 x 10^3	14730	2.9 x 10^3	2.8 x 10^3	1.3 x 10^2
Ni	15590	3.7 x 10^3	20070	3.9 x 10^3	3.8 x 10^3	1.6 x 10^2
Zn	3268	7.8 x 10^2	4938	9.7 x 10^2	8.7 x 10^2	1.3 x 10^2
Cu	12290	2.9 x 10^3	19920	3.9 x 10^3	3.4 x 10^3	6.9 x 10^2
As	7689	1.8 x 10^3	941	1.8 x 10^2	1.0 x 10^3	1.2 x 10^3
Se	331	7.9 x 10^1			7.9 x 10^1	-
Sr	794	1.9 x 10^2	778	1.5 x 10^2	1.7 x 10^2	2.6 x 10^1
Ag	10.9	2.6 x 10^0	17	3.3 x 10^0	3.0 x 10^0	5.2 x 10^{-1}
Cd	160	3.8 x 10^1	123	2.4 x 10^1	3.1 x 10^1	9.9 x 10^0
Cs	21.1	5.0 x 10^0	4.1	8.0 x 10^{-1}	2.9 x 10^0	3.0 x 10^0
Ba	1248	3.0 x 10^2	703	1.4 x 10^2	2.2 x 10^2	1.1 x 10^2
Pb	2099	5.0 x 10^2	1821	3.6 x 10^2	4.3 x 10^2	1.0 x 10^2
U238	13260	3.2 x 10^3	16790	3.3 x 10^3	3.2 x 10^3	9.7 x 10^1
P	**193200**	**4.6 x 10^4**	**181400**	**3.6 x 10^4**	**4.1 x 10^4**	**7.4 x 10^3**
S			**69720**	**1.4 x 10^4**	**1.4 x 10^4**	-
Ti	3084	7.3 x 10^2	6477	1.3 x 10^3	1.0 x 10^3	3.8 x 10^2
Zr	804	1.9 x 10^2	1076	2.1 x 10^2	2.0 x 10^2	1.4 x 10^1
Mo	4571	1.1 x 10^3	5827	1.1 x 10^3	1.1 x 10^3	3.9 x 10^1
Pd	628	1.5 x 10^2	675	1.3 x 10^2	1.4 x 10^2	1.2 x 10^1
Sn	928	2.2 x 10^2	1517	3.0 x 10^2	2.6 x 10^2	5.4 x 10^1
W	122	2.9 x 10^1	221	4.3 x 10^1	3.6 x 10^1	1.0 x 10^1
Th230	6.64	1.6 x 10^0	6.86	1.3 x 10^0	1.5 x 10^0	1.7 x 10^{-1}
Th232	9053	2.2 x 10^3	7292	1.4 x 10^3	1.8 x 10^3	5.1 x 10^2
U235	94.6	2.3 x 10^1	122	2.4 x 10^1	2.3 x 10^1	1.0 x 10^0

V. GENERAL DISCUSSION

The Silo 3 material is heterogeneous at submicron-level, yet reasonably uniform at the macroscopic level. This makes characterization with AEM an ideal method for investigating the form of the material. The AEM images and analysis reveal a material which is extremely fine-grained and diverse in composition and morphology. Many of the particles consist of tenacious agglomerates of particles, where compounds are encapsulated by others. The actinide-bearing particles were often in the colloidal-size range (i.e. < 0.5 μm) and exist as phosphates, silicates, and oxides. A significant fraction of the uranium in the sample is also associated with the hematite.

In Table V.1, the identifications are reported for all phases. In most cases a mineral name has been used to refer to a particular phase. Although, the compounds in Silo 3 cannot be called minerals (because minerals imply natural origins); the nomenclature is useful for describing phases which have complex chemical formulae. For example, fairfieldite minerals may contain different cations, such as transition metal ions, ammonium ions, Mg, or Ca in various amounts. The phosphate group may also exchange for arsenate in the phase. This properities of the mineral phases makes a quantitative analysis of the distribution of phases extremely difficult.

Table V.1 Distribution of mineral phases as determined with a AEM and XRD.

Identified phase	Mineral name	Mineral group	Comments
$CaSO_4$	anhydrite	anhydrite	euhedral particles 200-500 μm
$Fe_2(SO_4)_3$	kornelite		
$(Mg,Fe,Ca)_2(PO_4)_3$	fairfieldite	fairfieldite	anhedral
$CuFe_6(PO_4)_4(OH)_8$	chalcosiderite	turquoise	cryptocrystalline
$PbFe_3(PO_4)(SO_4)(OH)_6$	corkite	alunite	cryptocrystalline
$(Fe,Mg)(PO_4)(AsO_4)$	aresenates		cryptocrystalline
Fe_2O_3	hematite	corundum	cryptocrystalline and euhedral particles.
SiO_2	quartz	quartz	10-20 μm euhedral particles
Al_2O_3	corundum	corundum	euhedral crystals
$(Fe,Mg,Ca)SiO_x$	none		
$FeSiO_x$			amorph & xtals
$KAlSiO_x$	illite	mica	subhedral
$CaSiO_x$	wollastonite	pyroxenoid	

Mo-Vanadates			subhedral xtals
PbO_2	plattnerite	rutile	anhedral
Nd-La phosphate	brabantite	monazite	<50 nm
SnO_2	cassiterite	rutile	anhedral
Actinide-bearing phases			
Mg-uranyl silicate	sklodowskite	uranophane	< 50 nm
Mg-uranyl phosphate	saleeite	autunite	<200 nm
thorium oxide	thoria		< 10 nm
thorium phosphate			--
thorium iron silicate	hutonite		<10 nm
uranium oxide	uraninite	fluorite	

The phase abundance might be estimated using both the wet chemical analysis and the identification of the major phases. Some general observations based on the microscopic characterization may be valid. For instance most of the silicon appears to reside in quartz (SiO_2). Although some iron silicates and calcium silicates were found, but these seem to be minor components. Calcium is present in both anhydrite and phosphate phases. Most of the aluminum is in corrundum, and the magnesium is present mainly as a phosphate phase. The anions sulfur and phosphorous are present in a number of phases. It is important to note that not all the sulfur is present as anhydrite.

As no single element is unique to any one phase, efforts to material balance the results remain extremely hazardous; nevertheless, with the aid of the microanalysis, it has been possible to determine the compositions of many of the phases. Phases containing nitrogen and carbon were not identified uniquely. The XRD analysis suggested that the nitrogen was present as $NaNO_3$, but this was not confirmed by any of the other techniques. The major sodium-bearing phase was also not identified.

It is entirely possible that some phases were missed during the microscopy study. However, after repeated microscopic analyses using different samples from the original sample received from NFS, the same types of phases were re-appearing. This suggests that a representative sampling of the phases was obtained. In order to improve confidence in the data it woud be necessary to perform further AEM analyses. There will always be a degree of microscopist bias in any study using similar methods as this one. However, given the nature of the sample, its mix of amorphous, cryptocrystalline, and crystalline materials, varying density and particle size, the technique chosen may be the best comprise available to obtain a semi-quantitative distribution of the component compounds.

CONCLUSIONS

Owing to the complex nature of the Silo 3 material, we found that the macroscopic analysis could only be understood with the aid of detailed transmission electron microscopy investigation of the material. No other technique is available which can provide this type of information. The TEM information enabled the data from the XRD and from other techniques to be interpreted as much as possible. There are other techniques that might be useful for obtaining specific information on certain phases in the soils. Techniques which probe the nature of specific elements, such as extended fine structure X-ray absorption spectroscopy or nuclear magnetic resonance (with sulfur or carbon) may provide information on the local chemical environment of some elements (i.e. oxidation state and coordination number).

SUMMARY AND RECOMMENDATIONS

This study has revealed that the Silo 3 material is extremely complex; however the major phases are, calcium sulfate, magnesium and calcium phosphates, iron phosphates, iron oxides, and silicon dioxides. Many key elements are present in several forms and as oxides. The sulfur present in the Silo 3 wastes may present a problem for vitrification. Elimination of anhydrite from the waste will not remove all sulfur from the Silo 3 material. There is still a fraction of sulfur present in phosphates and in iron-bearing compounds.

REFERENCES

BUCK, E. C., DIETZ, N. L., and BATES, J. K. (1995) Uranium-contaminated soils: ultramicrotomy and electron beam analysis. *Micro. Res. Techniq.* **31**, 174-181.

BUFFLE, J. and LEPPARD, G. G. (1995) Characterization of aquatic colloids and macromolecules. 2. Key role of physical structures on analytical results. *Environ. Sci. Technol.* **29**, 2176-84.

EGERTON, R. F. (1986) Electron energy-loss spectroscopy (Plenum Press, New York).

EPA (1992) OSWER, Characterization protocol for radioactive contaminated soils, *U. S. EPA office of Solid Waste and Emergency Response*, Washington, D.C. Publication 9380.1-10FS.

GOLDSTEIN, J. I. and JOY, D. C. (1979) Introduction to analytical electron microscopy (Plenum Press, New York).

LORETTO, M. H. (1984) Electron beam analysis of materials (Chapman and Hall, London).

NEIHEISEL, J. (1992) Petrographic methods in characterization of radioactive and mixed Waste, HMC/Superfund '92, p192,December 1-3.

Appendix

A.1 Analysis from Nuclear Fuel Services

SUMMARY TABLE

ELEMENT	CONCENTRATION (ppm)	ACTIVITY (pCi/g)
Arsenic	938	NA
Barium	278	NA
Cadmium	23	NA
Lead	2380	NA
Selenium	29	NA
Silver	6	NA
Chromium	219	NA
Aluminum	19809	NA
Iron	52200	NA
Calcium	33400	NA
Sodium	9380	NA
Sulfur	60000	NA
Silicon	65333	NA
Magnesium	60298	NA
Phosphorus	40606	NA
Nitrogen	15296	NA
Carbon	5182	NA
Th-228	NA	747
Th-230	NA	60200
Th-232	NA	842
U-234	NA	1730
U-235/236	NA	117
U-238	NA	1780
Pb-210	NA	3480
Pb-211	NA	300
Pb-214	NA	1950
Ra-223	NA	400
Ra-224	NA	367
Ra-226	NA	3870
Ra-228	NA	406
Bi-214	NA	1800
Pa-231	NA	627
Rn-219	NA	175
Ac-227	NA	925

A.2 Scope of Work

SCOPE OF WORK

INTRODUCTION

Fluor Daniel Fernald is currently evaluating options for the remediation of Operable Unit 4 Silo 3 contents, composed primarily of calcined (kiln-dried) K-65 material. The purpose of these analyses is to identify the primary compounds in the silo material.

SCOPE

The material provided for analysis will be aliquoted from a sample of Silo 3 material previously shipped from Nuclear Fuel Services, Inc., in Erwin, Tennessee to Argonne National Laboratory. A representative fraction of at least 30 grams (but less than 100 grams) will be sent to Argonne for the following analyses:

1) Preliminary Optical Microscopy (OM). The sample will be prepared for a preliminary examination by scanning electron microscopy (SEM) to provide basic information on material composition.

2) Qualitative Elemetal Analysis. Although a good deal of information will be obtained from the preliminary OM, it will also be necessary to provide analysis with techniques which have greater sensitivity. Following the initial OM examination, epoxy mounts will be prepared for analysis by SEM and X-ray energy dispersive spectroscopy (EDS) to allow qualitative determination of the elemental composition of the individual phases and compounds.

3) Semi-Quantitative Characterization. Photography and X-ray diffraction will be used to make a determination of the percentage of each compound in the sample. Individual phases will be characterized with analytical transmission electron microscopy (AEM) combined with EDS and electron energy loss spectroscopy (EELS). Particles of the sample will be isolated and thin-sectioned for further examination with AEM.

DELIVERABLES

1) Results from the various analytical techniques will be combined to give best estimate as to identity and concentration of compound types.
2) A brief summary of the analytical methods used to generate the data.
3) Copies of applicable raw data.
4) Recommendations for additional work.
5) The analytical data package should be shipped to:

Shipping Address:
Denise Arico
UNO Building
11003 Hamilton Cleves Rd.
Ross, Ohio 45061

Mailing Address:
Denise Arico
Fluor Daniel Fernald - MS90
P.O. Box 538704
Cincinnati, Ohio 45253-8704

SAFETY

The material should be treated with caution. Appropriate radiological controls should be in place. Furthermore, since the samples have a significant amount of uranium and emit radon, they should be handled in a hood.

Argonne National Laboratories
Statement of Work for
Additional Analysis on the
Silo 3 Compound Analysis

April 29, 1997

1. The Silo 3 material will be dissolved by with the appropriate mineral acid in a Teflon beaker on a hot plate and taken to dryness. Samples will be fumed with $HClO_4$ to insure complete dissolution of actinides, dissolved in 1 ml HCl and diluted to 100 ml.. Any insoluble material will be removed by filtration, quantitated and retained prior to final volume adjustment. Insoluble material will be analyzed at the direction of FDF.

2. A second dissolution will be preformed for Si and volatile element analysis. Any insoluble material will be removed by filtration, quantitated and retained prior to final volume adjustment. Insoluble material will be analyzed at the direction of FDF.

3. Elemental determination will be preformed by using ICP-MS for constituents above 0.1 wt.%.

4. Radionuclide content will be determined by gamma spectrometry.

5. Thorium-230 content will be determined via alpha spec.

6. Sample will be analyzed for sulfite, sulfate, phosphate, and nitrate.

7. Vendor will provide methods for these analysis to FDF, prior to start of these analysis.

A.4 X-ray diffraction data

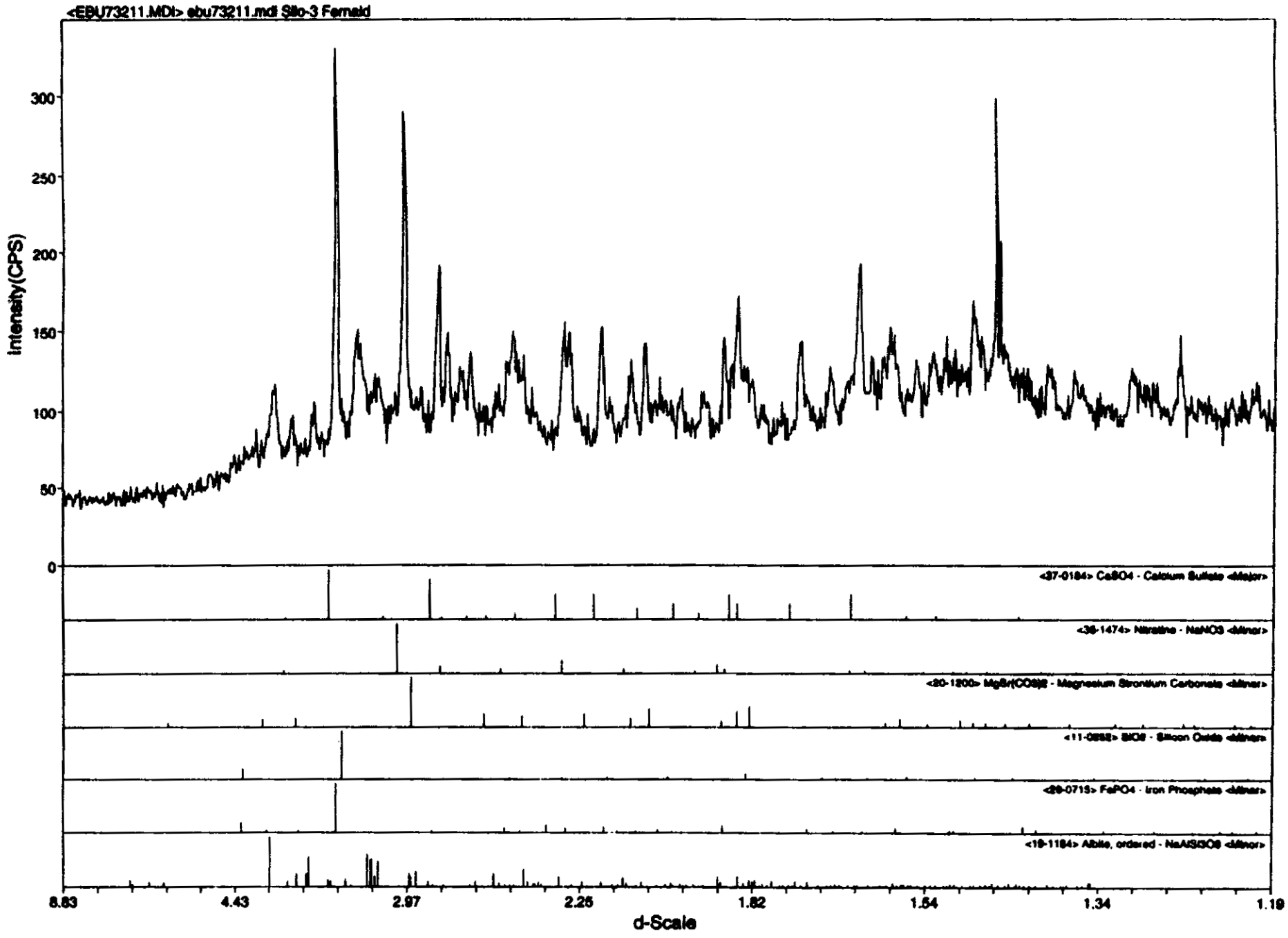
<EBU73211.MDI> ebu73211.mdi Silo-3 Fernald
Intensity(CPS)
300
250
200
150
100
50
0
<37-0184> CaSO4 - Calcium Sulfate <Major>
<36-1474> Nitratine - NaNO3 <Minor>
<20-1200> MgSr(CO3)2 - Magnesium Strontium Carbonate <Minor>
<11-0682> SiO2 - Silicon Oxide <Minor>
<29-0715> FePO4 - Iron Phosphate <Minor>
<19-1184> Albite, ordered - NaAlSi3O8 <Minor>
8.83
4.43
2.97
2.25
1.82
1.54
1.34
1.19
d-Scale

T/ACL

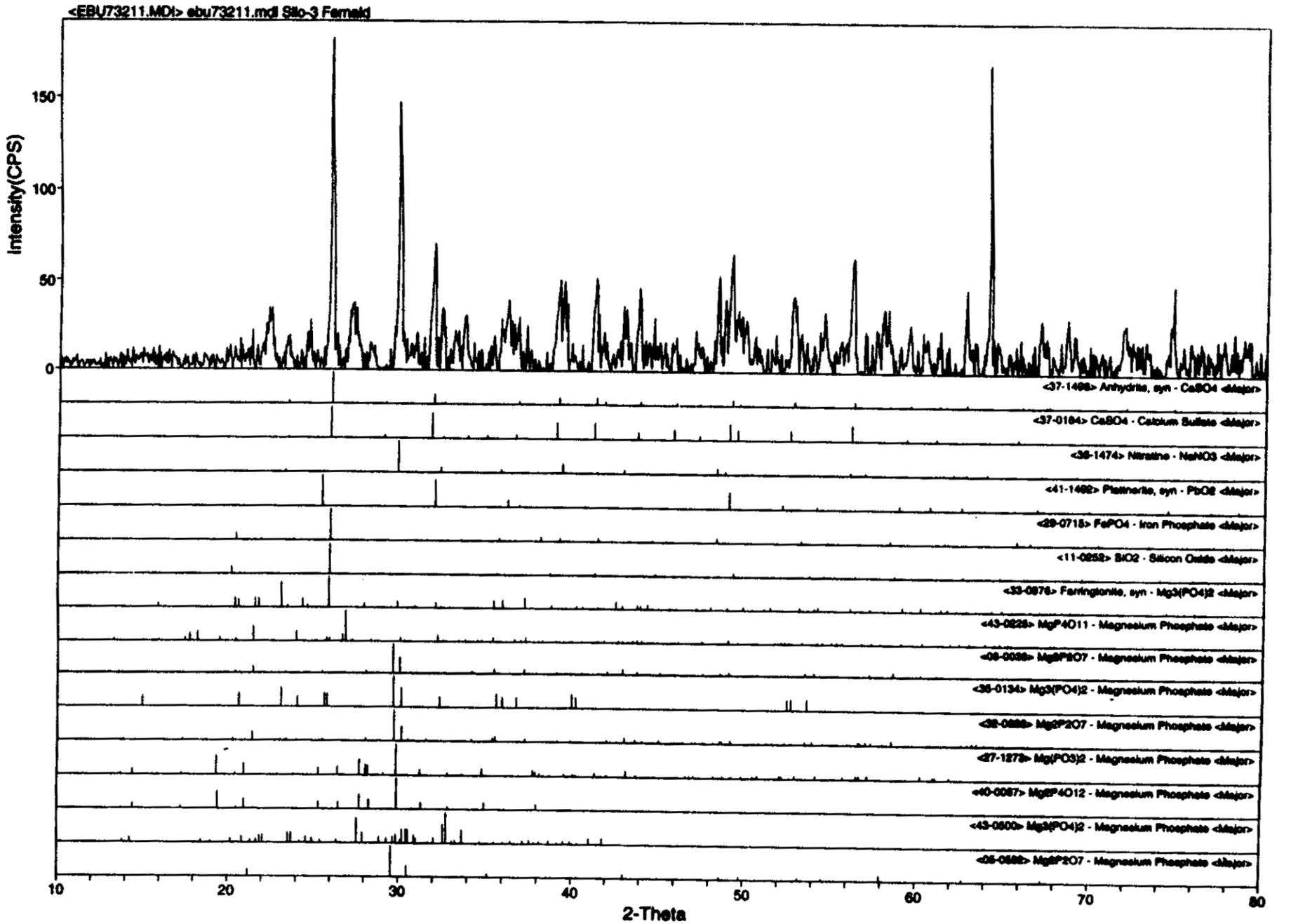

T/ACL

<c:\jade\data97> Thursday, Apr 03, 1997 @11:28a

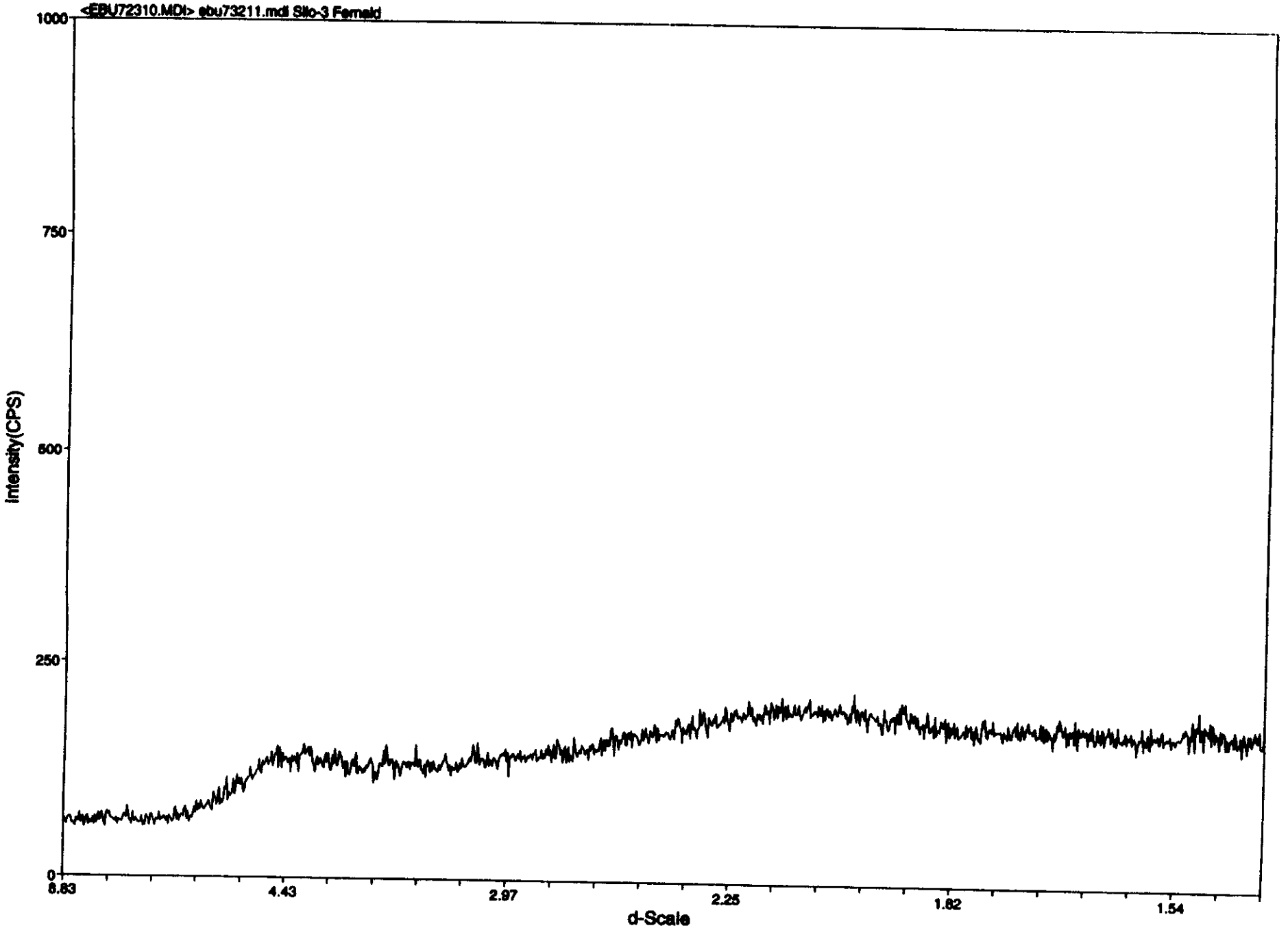
<EBU72310.MDI> ebu73211.mdl Silo-3 Ferneid
1000
750
500
250
0
Intensity(CPS)
8.83
4.43
2.97
2.25
1.82
1.54
d-Scale

T/ACL

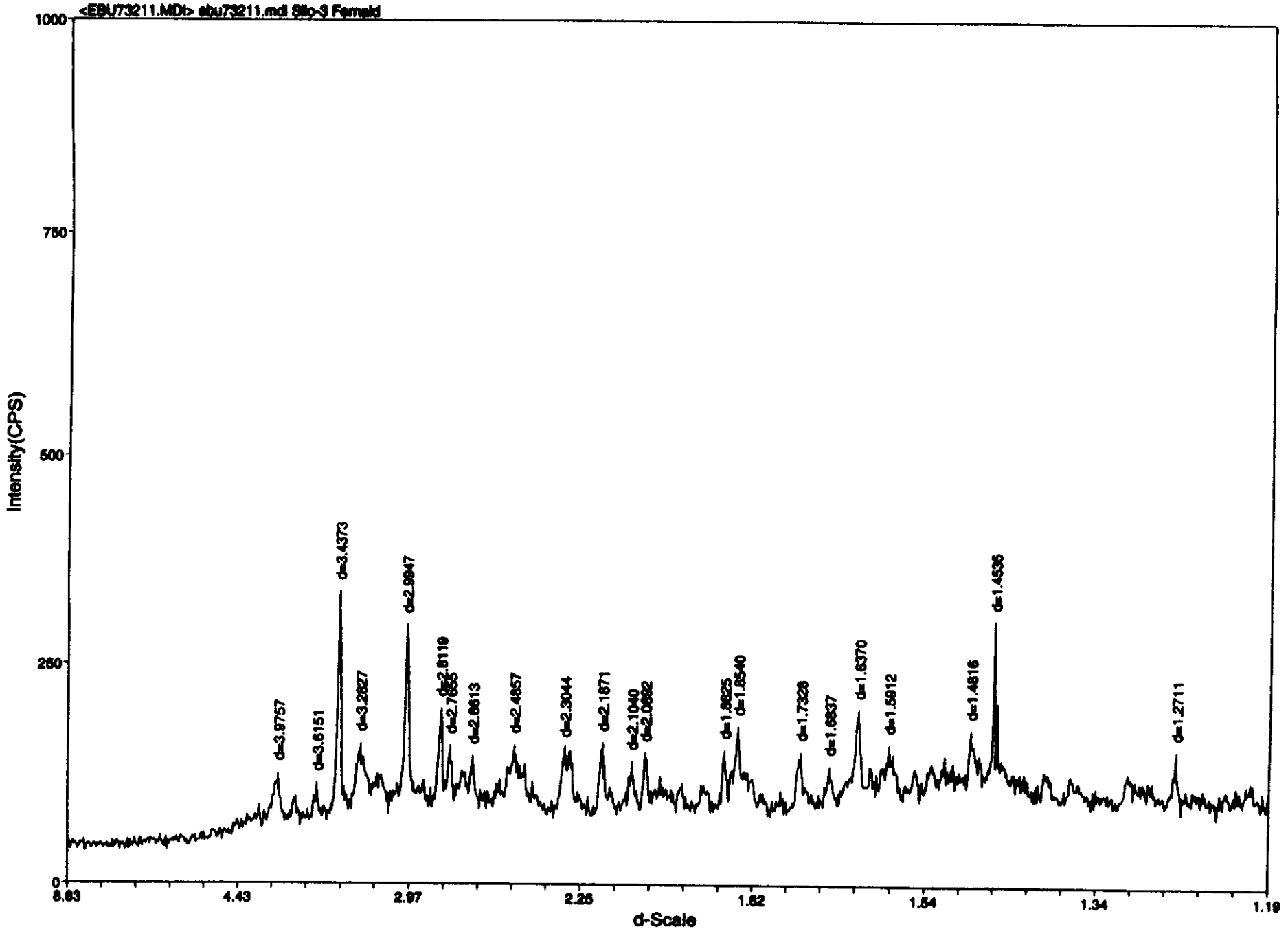

MT/ACL

<c:\jade\data97> Friday, Apr 04, 1997 @08:54a

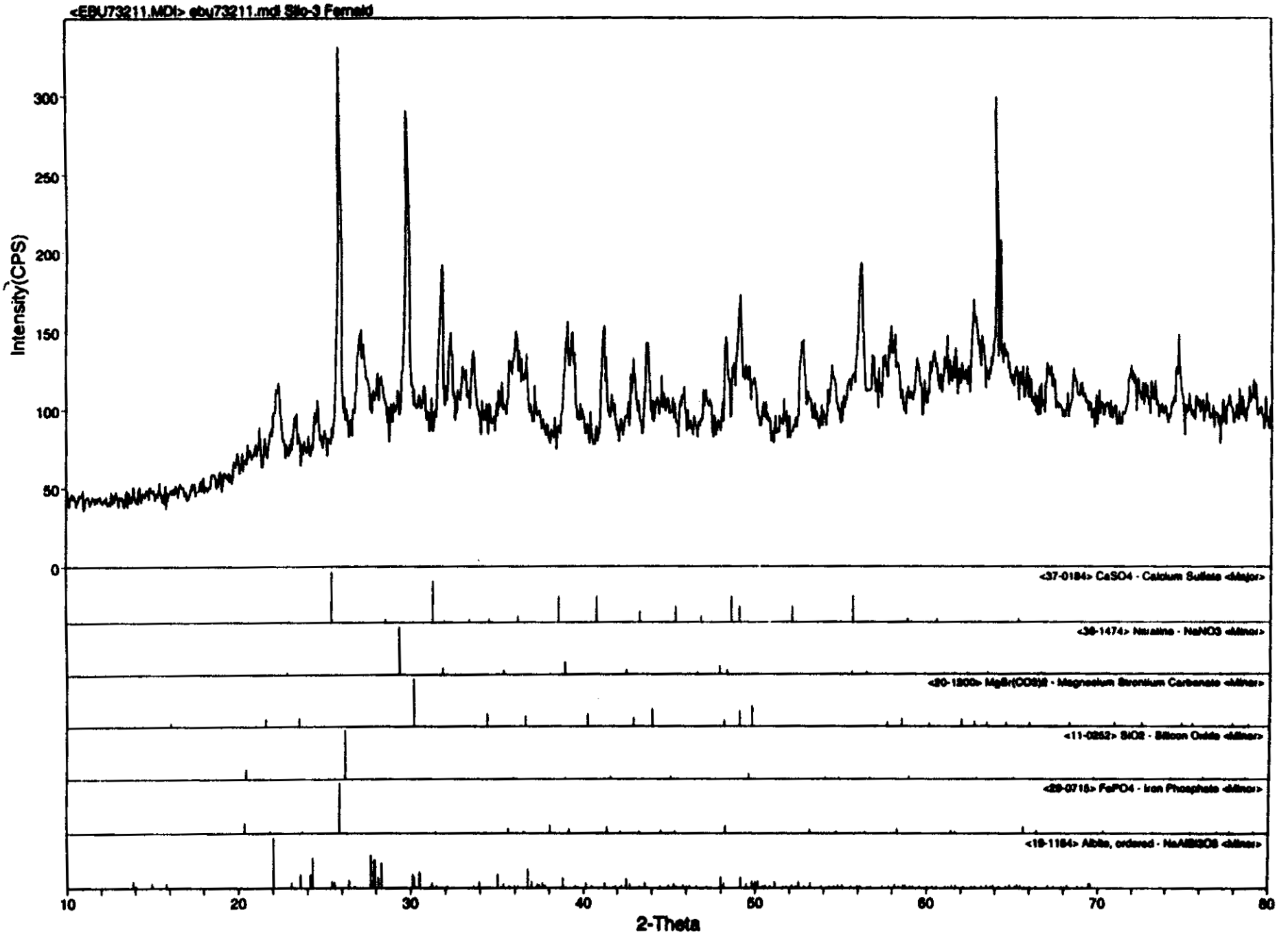
<EBU73211.MDI> ebu73211.mdi Silo-3 Fernald
Intensity(CPS)
300
250
200
150
100
50
0
<37-0184> CaSO4 - Calcium Sulfate <Major>
<36-1474> Nitratine - NaNO3 <Minor>
<20-1300> MgSr(CO3)2 - Magnesium Strontium Carbonate <Minor>
<11-0252> SiO2 - Silicon Oxide <Minor>
<29-0715> FePO4 - Iron Phosphate <Minor>
<19-1184> Albite, ordered - NaAlSi3O8 <Minor>
10
20
30
40
50
60
70
80
2-Theta